eIF2B localization and its regulation during the integrated stress response is cell-type specific

HANSON, Filipe, RIBEIRO DE OLIVEIRA, Madalena, CROSS, Alison <http://orcid.org/0000-0003-0655-6993>, ALLEN, Liz <http://orcid.org/0000-0001-8579-7730> and CAMPBELL, Susan <http://orcid.org/0000-0002-6740-1445>

Published version

HANSON, Filipe, RIBEIRO DE OLIVEIRA, Madalena, CROSS, Alison, ALLEN, Liz and CAMPBELL, Susan (2024). eIF2B localization and its regulation during the integrated stress response is cell-type specific. iScience, 27 (9): 110851. [Article]

iScience

CellPress
OPEN ACCESS

Article

eIF2B localization and its regulation during the integrated stress response is cell-type specific

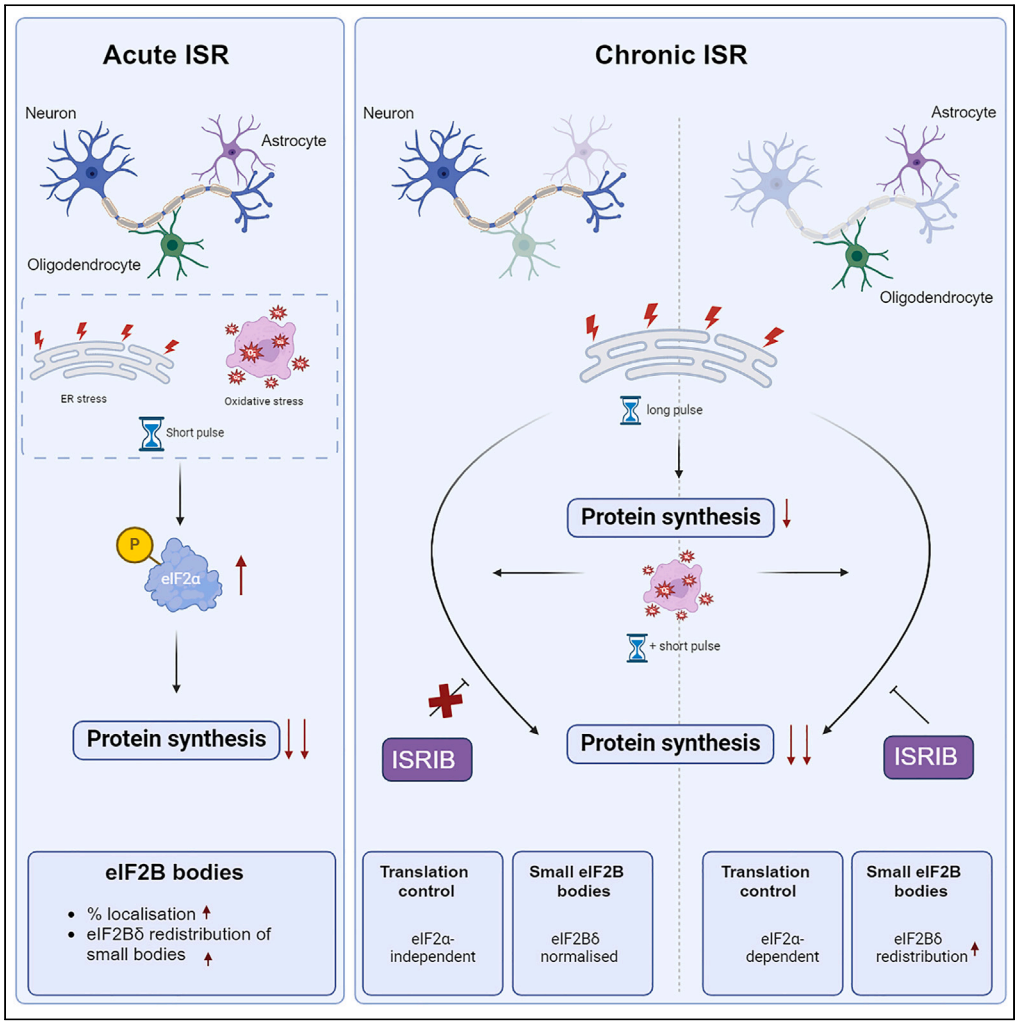

Filipe M. Hanson, Madalena I. Ribeiro de Oliveira, Alison K. Cross, K. Elizabeth Allen, Susan G. Campbell

susan.campbell@shu.ac.uk

Highlights

eIF2B localization ("eIF2B bodies") is cell-type specific

Chronic ISR primes cell-specific control of translation

Regulation of eIF2B bodies correlates with cell-specific translational control

ISRIB shows cell type specificity during chronic ISR

Hanson et al., iScience 27, 110851
September 20, 2024
https://doi.org/10.1016/j.isci.2024.110851

iScience

CellPress
OPEN ACCESS

Article

eIF2B localization and its regulation during the integrated stress response is cell-type specific

Filipe M. Hanson,[1] Madalena I. Ribeiro de Oliveira,[1] Alison K. Cross,[1] K. Elizabeth Allen,[1] and Susan G. Campbell[1,2,*]

SUMMARY

Eukaryotic initiation factor 2B (eIF2B) controls translation initiation by recycling inactive eIF2-GDP to active eIF2-GTP. Under cellular stress, the integrated stress response (ISR) is activated inhibiting eIF2B activity resulting in the translation attenuation and reprogramming of gene expression to overcome the stress. The ISR can dictate cell fate wherein chronic activation has pathological outcomes. Vanishing white matter disease (VWMD) is a chronic ISR-related disorder with mutations in eIF2B targeting astrocyte and oligodendrocyte cells. Regulation of eIF2B localization (eIF2B bodies) has been implicated in the ISR. We present evidence that neuronal and glial cell types possess distinct patterns of eIF2B bodies which change in a manner correlating to acute and chronic ISR activation. We also demonstrate that while neural and glial cell types respond similarly to the acute induction of the ISR a chronic ISR exerts cell-type specific differences. These findings provide key insights into neural cell responses and adaptation to cellular stress.

INTRODUCTION

All biological processes are intrinsically dependent upon the highly conserved and hierarchical process of mRNA translation. A key protein complex involved in ensuring that efficient translation initiation takes place is the eukaryotic initiation factor 2, eIF2. eIF2 is a heterotrimeric G-protein made up of the subunits α, β, and γ.[1,2] In its active GTP-bound state, eIF2 is complexed with initiator methionyl tRNA (eIF2-GTP-Met-tRNAi) and forms a ternary complex (TC) whose key role is to locate the first start codon to the ribosome.[3] Following codon recognition, eIF2-GTP is hydrolyzed to eIF2-GDP through the action of the canonical GTPase-activating protein eIF5.[4] Crucial for successive rounds of translation is the regeneration of GTP-bound eIF2 which is catalyzed by the guanine nucleotide exchange factor (GEF) eIF2B. Once released from the scanning ribosome, eIF5 stays associated with eIF2-GDP and hinders any spontaneous GDP release (GDP dissociation inhibitor, GDI) from eIF2. In addition to its GEF function, eIF2B acts as a GDI displacement factor,[5] removing eIF5, followed by GDP release from eIF2.[6] These functions highlight eIF2B as a powerful control checkpoint for the availability of TCs.

In its native form, eIF2B is a heterodecameric complex composed of two copies of 5 non-identical subunits (termed eIF2Bα-ε). The γ and ε subunits catalyze the GEF activity, whereas the α, β and δ subunits regulate this activity in response to different cellular stress insults.[7–10] Structurally, eIF2B decameric conformation is comprised of an eIF2B$(\alpha\beta\delta)_2$ hexameric regulatory core laid between two eIF2B(γε) catalytic heterodimers.[11,12] In mammalian cells, eIF2B has been reported to exist in different sub-complexes arrangements with varying subunit composition.[13,14]

At the hub of translational control is the regulation of eIF2B activity by the integrated stress response (ISR).[15,16] During acute or transient stress, the ISR activates stress-sensing kinases (PERK, PKR, GCN2, HRI) which phosphorylate the α subunit of eIF2 at serine 51 (eIF2α-P[S51]). Phosphorylated eIF2α acts as a competitive substrate to its unphosphorylated cognate, blocking GEF activity of decameric eIF2B by inhibiting the interaction of eIF2γ with the eIF2Bε subunit.[17–22] Attenuated eIF2B activity limits TC levels and reduces global protein synthesis. Concomitantly, a specific subset of mRNAs harboring upstream ORFs bypasses this translation attenuation. These include activating transcription factor 4, ATF4, and C/EBP homologous protein, CHOP.[23] In contrast, transition to a chronically activated ISR is widely reported as adaptive to prolonged stress, ultimately pro-apoptotic when cells are unable to overcome sustained stress with pathological consequences.[24]

In yeast cells, eIF2B localizes to stable cytoplasmic foci termed "eIF2B bodies" where GEF activity takes place and is targeted for regulation.[25–31] These studies were further extended in mammalian cells where heterogeneous populations of different-sized bodies correlating to their eIF2B subunit makeup were observed.[32] Larger bodies contained all eIF2B subunits, whilst small bodies predominantly consisted of the γ and ε catalytic subunits. Upon acute endoplasmic reticulum (ER) stress, it was demonstrated that the ISR differentially modulates these eIF2B

[1]Biomolecular Sciences Research Centre, Industry and Innovation Research Institute (I[2]RI), Sheffield Hallam University, Sheffield S1 1WB, UK
[2]Lead contact
*Correspondence: susan.campbell@shu.ac.uk
https://doi.org/10.1016/j.isci.2024.110851

body subpopulations, decreasing the GEF activity of larger bodies and inversely increasing GEF activity within small bodies. This increase in GEF activity was concomitant with a redistribution of eIF2Bδ to small bodies, suggesting the existence of a previously unidentified eIF2Bγδε heterotrimeric sub-complex. ISR-targeting drugs (e.g., ISRIB) which boost translation, recapitulated this eIF2Bδ redistribution to small bodies in unstressed cells,[32] thus implying that this action might be an innate response to the ISR to allow low baseline levels of translation. Nonetheless, the functional relevance of eIF2Bδ redistribution is still unknown.

Despite eIF2B's ubiquitous role in the ISR across all cell types,[15] mutations in any of the five subunits of eIF2B result in the neurological disorder leukodystrophy with vanishing white matter disease (VWMD).[33] VWMD mutations are selectively detrimental to astrocytes, cause defective maturation and mitochondrial dysfunction in oligodendrocytes and, ultimately, lead to neuronal death due to axonal demyelination.[34–39] Surprisingly, studies have shown that cultured neurons are unaffected by eIF2B VWMD mutations, implying that cell-type specific features of eIF2B function and regulation may exist at least in brain cell types, which remains to be understood. We previously showed that eIF2B bodies are sites of eIF2B GEF activity as eIF2 can shuttle into these bodies in a manner that correlates with ISR activation.[32] Here, we investigated steady-state eIF2B localization dynamics and subsequent changes upon cellular stress and classical ISR-targeting drugs in neuronal and glial cell lines. We report that eIF2B localization to eIF2B bodies is tailored in a cell-type specific manner. We also demonstrate that the regulatory composition of eIF2B bodies is tightly modulated by cellular stress in a cell-type manner. We further showcase a novel cell-type sensitivity feature of ISRIB in the regulation of eIF2B body composition and eIF2 shuttling.

RESULTS

Eukaryotic initiation factor 2B localizes to eukaryotic initiation factor 2B bodies in a cell type dependent manner

eIF2B localization has been reported in yeast[25,28,31] and, more recently, in mammalian cells [32] (Hodgson et al., 2019), however the latter shows a higher degree of complexity. To further our knowledge of cellular eIF2B localization, we transiently transfected the catalytic ε subunit (eIF2Bε) tagged with a monomeric green fluorescent protein (mGFP) into neuroblastoma (SH-SY5Y), astrocytoma (U373) and hybrid primary oligodendrocytes (MO3.13) cell lines and observed different patterns of eIF2B localization in all 3 cells lines (Figure 1A). Immunocytochemistry was also carried out to ensure that these cells expressed key cell type specific markers (Figure S1A) Cells expressing eIF2Bε-mGFP exhibited either eIF2B bodies or the localization was fully dispersed throughout the cytoplasm (Figure 1Bi). We observed that the percentage (%) of cells localizing eIF2B significantly differ across cell types (Figure 1Bii). U373 cells showed the highest percentage of cells containing eIF2B bodies (53.50%) followed by MO3.13 (33.25%) and SH-SY5Y exhibiting the lowest percentage (19.25%). Because eIF2B overexpression could potentially impact the observed localization pattern across cell types, we examined endogenous eIF2Bε and observed a similar trend (Figure S1B). Next, given the heterogeneous populations of different sized eIF2B bodies, we subcategorized them into small eIF2B bodies ($<1\mu^2$) or large eIF2B bodies ($\geq 1\mu^2$) (Figure 1C). Small eIF2Bε-mGFP bodies were the predominant subpopulation across all cell types. U373 and MO3.13 cells exhibited a similar percentage per cell (88.19% and 89.34%, respectively), and both were slightly higher in comparison to SH-SY5Y cells (71.46%). In contrast, SH-SY5Y cells displayed an increased average percentage of large eIF2Bε-mGFP bodies per cell (30.54%) in comparison to U373 and MO3.13 cells (13.81% and 12.66%, respectively). Here, we show that eIF2B localization is fundamentally cell type specific: each brain cell type harbors its own prevalence of eIF2B bodies although the abundance of each body size group is suggested to be similar amongst glial cell types.

Subunit composition of eukaryotic initiation factor 2B bodies is cell-type specific

eIF2B exists as a decameric complex. eIF2Bε alone can carry out GEF activity; however, the rate of this exchange is enhanced upon the joining of other eIF2B subunits.[40] Regulatory subunits increase GEF activity, modulate levels of eIF2B activity upon cellular stress and, more recently, co-localize to eIF2B bodies in a size-dependent manner.[13,32] Having shown that eIF2B localization is different between cell types (Figures 1B and 1C), we next investigated whether subunit co-localization to eIF2Bε-mGFP bodies also exhibits cell type specific features. We performed immunocytochemistry on the regulatory (eIF2Bα, eIF2Bβ, eIF2Bδ) and catalytic (eIF2Bγ) subunits of eIF2B in SH-SY5Y, U373 and MO3.13 cells (Figure 1Di). Previous data using U373 cells revealed that small eIF2B bodies predominantly contain catalytic subunits, while larger eIF2B bodies additionally contain a mixture of regulatory subunits.[32] We confirmed that this trend is observed across all cell types by measuring the percentage (%) of small and large eIF2Bε-mGFP bodies that co-localize with the remaining subunits (eIF2Bα-γ). eIF2Bγ co-localization with eIF2Bε-mGFP showed the highest mean percentage in small eIF2B bodies, although slightly increased in neuronal cells when compared to glial cells (SH-SY5Y: 51.99%; U373: 31.86%; MO3.13: 31.63%) (Figure 1Dii). Moreover, neuronal cells also displayed a significantly higher percentage of small bodies containing regulatory subunits eIF2Bα (SH-SY5Y: 27.58%; U373: 7.72%; MO3.13: 8.13%), eIF2Bβ (SH-SY5Y: 17.33%; U373: 5.94%; MO3.13: 0.68%) and eIF2Bδ (SH-SY5Y: 20.83%; U373: 10.63%; MO3.13: 9.03%). Large eIF2B bodies showed similar catalytic eIF2Bγ co-localization across all cell types (SH-SY5Y: 91.23%; U373: 93.22%; MO3.13: 77.02%) with drastic cell-type disparities on regulatory subunit make-up (Figure 1Dii). Oligodendrocytic cells displayed slightly lower eIF2Bα co-localization albeit no statistically significant difference compared to the other cell types (SH-SY5Y: 60.26%; U373: 59.02%; MO3.13: 38.25%) and near absence of eIF2Bβ co-localization (SH-SY5Y: 38.38%; U373: 41.13%; MO3.13: 0.62%) even though endogenous eIF2Bβ localizes to cytoplasmic foci (Figure 1Dii). eIF2Bδ co-localization to large eIF2B bodies was overall similar across cell types (SH-SY5Y: 62.39%; U373: 67.48%; MO3.13: 65.00%). These results demonstrate that our previous findings correlating eIF2B body size to subunit composition[32] is somewhat exerted on a cell type basis: astrocytic and neuronal cells follow this size:subunit pattern while eIF2B bodies of oligodendrocytes are largely depleted of a regulatory eIF2B subunit.

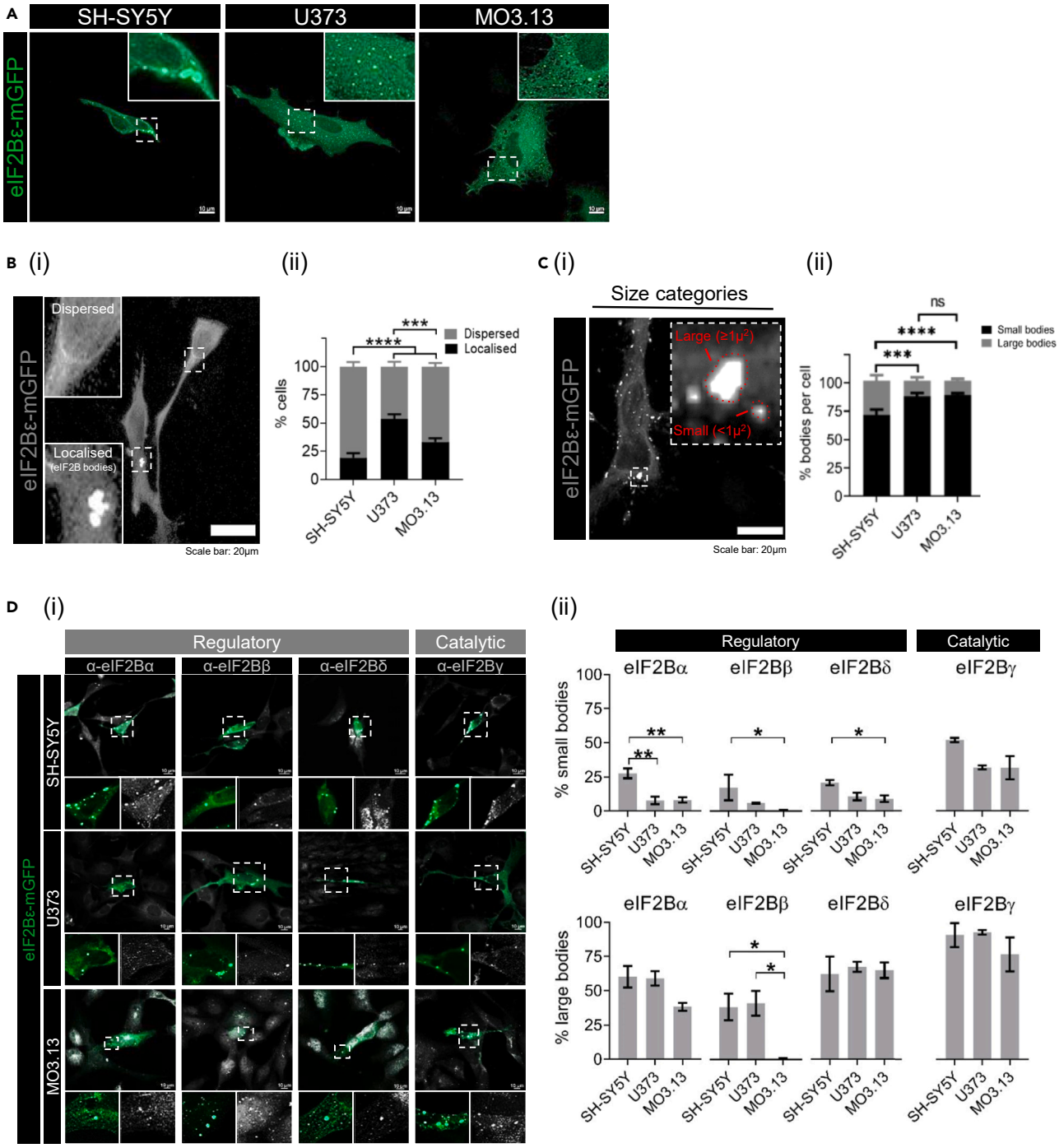

Figure 1. eIF2B localization is cell-type specific

(A) SH-SY5Y, U373, and MO3.13 cells subjected to transient transfection and expressing eIF2Bε-mGFP. Scale bar: 10 μm.

(B) (i) Cells express dispersed eIF2B or localized eIF2B (eIF2B bodies). (ii) Mean percentage of cells displaying dispersed eIF2B or localized eIF2B in a population of 100 transfected cells (mean ± SEM; $N = 4$; $^{****}p \leq 0.001$, $^{***}p \leq 0.001$ according to two-way ANOVA).

(C) (i) eIF2B bodies were categorized as small bodies ($<1\mu^2$) and large bodies ($\geq 1\mu^2$). (ii) Within the transfected cells exhibiting localized eIF2B, the mean percentage of small and large eIF2B bodies in a population of 50 cells (mean ± SEM; $N = 3$; $^{****}p \leq 0.001$, $^{***}p \leq 0.001$, *ns*: non-significant according to two-way ANOVA).

(D) (i) Confocal images of SH-SY5Y, U373 and MO3.13 expressing eIF2Bε-mGFP and immunolabelled with primary anti-eIF2Bα, anti-eIF2Bβ, anti-eIF2Bδ and anti-eIF2Bγ. Scale bar: 10 μm. (ii) Mean percentage of small (*top panel*) and large bodies (*bottom panel*) co-localizing with eIF2B(α-γ) subunits of at least 30 cells per repeat (mean ± SEM; $N = 3$; $^{**}p \leq 0.01$, $^{*}p < 0.05$ according to one-way ANOVA).

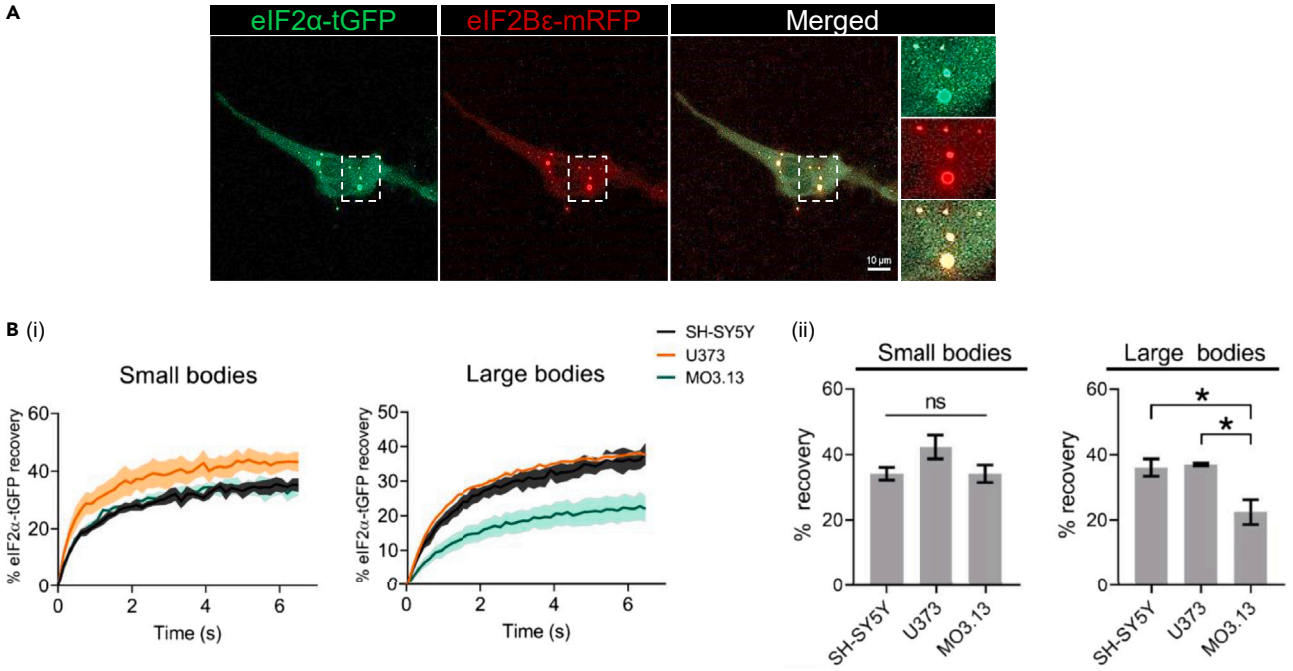

Figure 2. eIF2 shuttling of eIF2B bodies is cell-type specific

Cells were co-transfected with eIF2α-tGFP to carry out fluorescence recovery after photo bleaching (FRAP) analysis, and eIF2Bε-mRFP to locate the eIF2B body.

(A) Representative live cell imaging of a cell co-expressing eIF2α-tGFP and eIF2Bε-RFP. Scale bar: 10 μm.

(B) (i) Quantification of normalized FRAP curves for eIF2α-tGFP of at least 10 bodies of each size category of SH-SY5Y, U373, and MO3.13 cells. The data were graphed and shown as the mean and SEM bands (*N=3*). (ii) Mean percentage of eIF2α-tGFP recovery determined from normalized FRAP curves (mean ± SEM; *N* = 3; **p* < 0.05 according to one-way ANOVA).

The rate of eIF2 shuttling within eukaryotic initiation factor 2B bodies is cell-type specific

eIF2B controls the levels of ternary complexes by regulating the available pool of GTP-bound eIF2. Previous studies from our lab have shown that the shuttling rate of eIF2 through eIF2B bodies can infer eIF2B GEF activity.[25,26,29,32] We co-transfected eIF2α-tGFP and eIF2Bε-mRFP in SH-SY5Y, U373, and MO3.13 cells and performed fluorescence recovery after photobleaching (FRAP) on small and large eIF2B bodies. We first confirmed that all sized eIF2Bε-RFP bodies co-localized with eIF2α-tGFP (Figure 2A). Next, FRAP analysis showed that eIF2α-tGFP recovery of small eIF2B bodies was relatively similar across cell types, although slightly higher for U373 cells despite not being statistically significant (SH-SY5Y, 34.21%; U373, 42.32%; MO3.13, 34.16%) (Figures 2Bi and ii). Surprisingly, large eIF2B bodies showed drastic discrepancies. SH-SY5Y and U373 cells exhibited similar eIF2α-tGFP recovery (SH-SY5Y: 36.13%; U373: 37.08%) whilst MO3.13 cells have significantly lower recovery (22.51%) (Figure 2Bii). Hence, these data demonstrate that small eIF2B bodies displaying similar % recoveries are functionally similar across all cell types whilst large eIF2B bodies display cell type specific differences.

The acute integrated stress response is similar across cell types while chronic integrated stress response displays cell-type specific features

eIF2B localization is modulated upon the induction of an acute ISR in astrocytes.[32] Here we further characterized eIF2B localization during the transition to a chronic ISR by firstly characterizing the acute vs. chronic ISR activation in neuronal and glial cell types. To test the induction of the acute ISR we used thapsigargin (Tg) and sodium arsenite (SA) to trigger ER stress and oxidative stress, respectively (Figure 3A). We performed Western blot analysis using canonical ISR markers (PERK-P, eIF2α-P, CHOP, and GADD34) (Figure 3Bi). As expected, short-term treatment with either Tg (1 μM 1h) or SA (125 μM 0.5h) led to increased eIF2α phosphorylation (eIF2α-P) and eIF2α-P-dependent protein synthesis shutdown across all cell types (Figure 3Bii). Next, cells were exposed to Tg at a lower concentration (300 nM) for 24h to monitor ER stress during the chronic ISR adaptation phase[41] (Figure 3A). As expected, PERK remained partially phosphorylated (shifted PERK band) and ISR markers (CHOP, GADD34) were expressed (Figure 3Bi). ATF4 expression was no longer detected at the 24h time point, however temporal monitoring during this 24h period showed that it peaked at 4-8h post-Tg treatment across all cell types (Figure S2). A Tg treatment for 24h showed partial translation recovery in comparison to 1h Tg treatment, confirming the transition to a chronic ISR program.[42]

VWMD is predominantly characterized by an abnormal chronic-like ISR which selectively targets glial function exhibited by progressive white matter deterioration upon acute stress episodes (e.g., head traumas and infections). However, this glial vulnerability remains poorly understood. To provide insight into this cell type specificity, we devised a VWMD-mimicking environment in SH-SY5Y, U373, and MO3.13

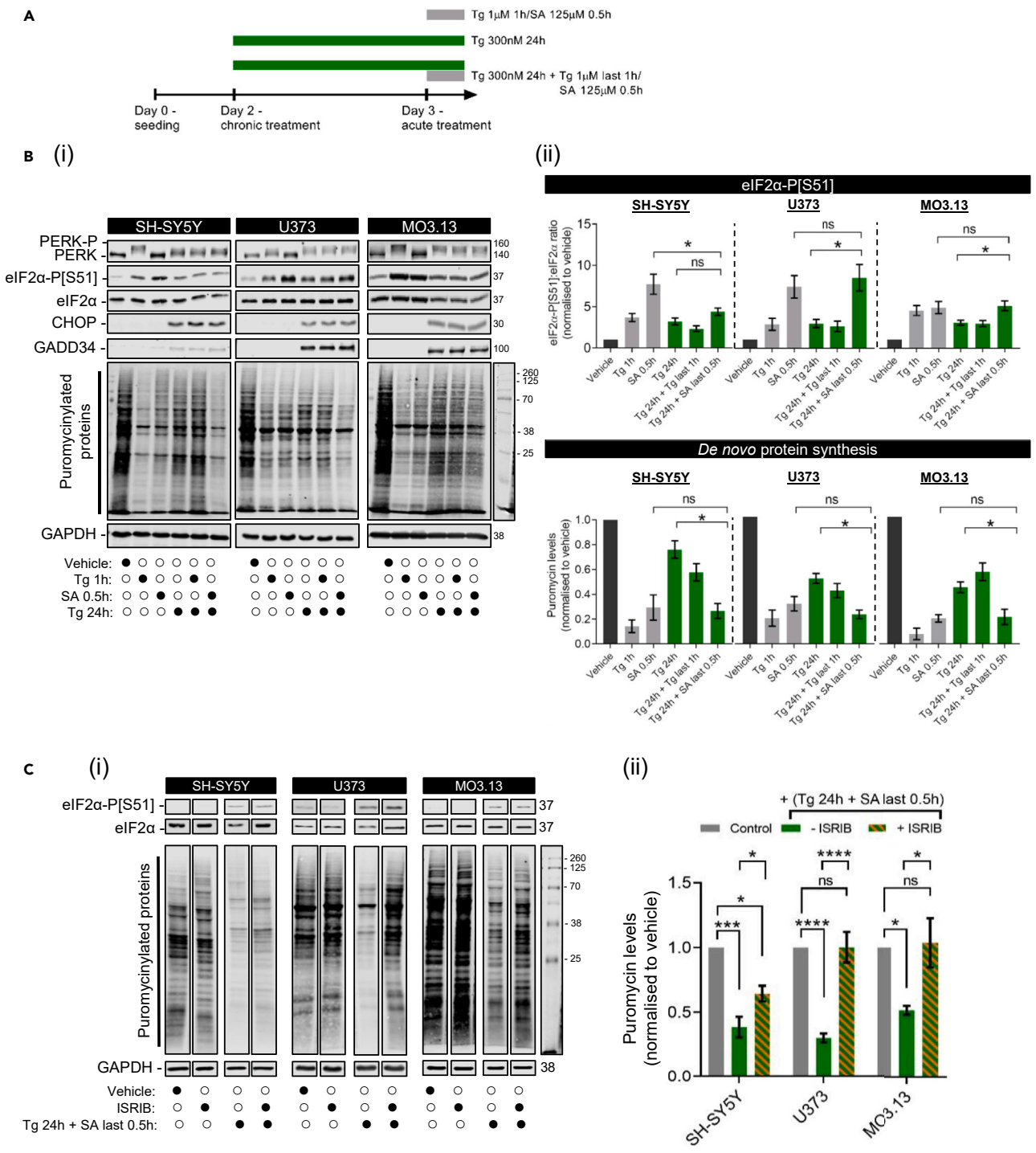

Figure 3. ER stress-preconditioned cells do not respond to additional acute ER stress treatment but do respond to acute oxidative stress in a cell type manner

(A) Schematic diagram of stress treatments.

(B) (i) Representative Western blot of the ISR expression profile (PERK-P, PERK, eIF2α-P[S51], pan-eIF2α, CHOP, and GADD34) and global newly synthesized proteins (puromycin incorporation assay) in SH-SY5Y, U373 and MO3.13 cells treated with vehicle (DMSO), acute stress inducers (Tg 1 μM for 1h and SA 125 μM for 30 min) or chronic ER stress (Tg 300 nM for 24h) subsequently challenged with previously described acute stress treatments. (ii) Mean expression levels of eIF2α-P[S51] normalized to total eIF2α levels (*top panel*) and puromycin-labeled nascent proteins normalized to housekeeping GAPDH levels (*bottom panel*) upon the previously described stress conditions. Fold-change relative to vehicle-treated cells was calculated and analyzed using one-way ANOVA (mean ± SEM; $N = 3–9$; $*p < 0.05$, *ns*: non-significant). Chronic ER stress conditions are highlighted in green.

Figure 3. *Continued*

(C) (i) Representative Western blot of eIF2α-P[S51], pan-eIF2α, and global newly synthesized proteins (puromycin incorporation assay) in SH-SY5Y, U373, and MO3.13 cells treated with ISRIB (200nM) for 1h alone, Tg 300 nM for 24h added with SA 125 μM in the last 30min, or combination of both. DMSO for 24h was used as a vehicle. (ii) Mean expression levels of puromycin-labeled nascent proteins normalized to housekeeping GAPDH levels. Fold-change relative to vehicle-treated cells was calculated and analyzed using one-way ANOVA (mean ± SEM; $N = 3–4$; ****$p \leq 0.001$, ***$p \leq 0.001$, *$p < 0.05$, *ns*: non-significant).

cells whereby cells exposed to a chronic ISR are subsequently exposed to an acute insult. Cells were treated with 300 nM Tg for 24h and then 1 μM Tg or 125 μM SA in the final 1h or 30 min, respectively. Interestingly, the additional Tg treatment did not affect ISR markers nor translation levels, suggesting that an ongoing chronic ER stress is protective against a new ER stress insult (Figures 3Bi and ii). To confirm that this observed unresponsiveness was not due to Tg saturation or ISR-independent cellular effects of Tg, we treated cells with tunicamycin (Tm; which inhibits the *N*-linked glycosylation of ER proteins and leads to an ER stress activated ISR like Tg) in the last 2h of a 24h treatment with 300 nM Tg. Tm treatment alone induced eIF2α phosphorylation and suppressed protein synthesis, while the additional Tm treatment to Tg preconditioned cells did not further impact protein synthesis when compared to Tg 24h alone (Figure S3). However, when the cells were subsequently treated with acute oxidative stress (SA: 125 μM 0.5h), a decrease in *de novo* protein synthesis akin to SA-only levels was observed (Figure 3Bii), suggesting that cells reset the acute ISR program following chronic ER stress when exposed to different stressors. This decrease in protein synthesis was linked to a significant increase in eIF2α phosphorylation in U373 and MO3.13 cells. Unexpectedly, this eIF2α phosphorylation increase was not as dramatic in SH-SY5Y cells; suggesting that the suppression of protein synthesis observed here may be less dependent on eIF2α phosphorylation (Figure 3Bii). To test whether this was the case, we employed the same chronic stress conditions (Tg 24h, Tg 24h + Tg last 1h; Tg 24h + SA last 0.5h) in the presence or absence of the ISR inhibitor ISRIB (last 1h) and performed puromycin incorporation assay (Figure 3C). ISRIB which reverses the inhibitory effects of eIF2α phosphorylation[43] was unable to fully restore protein synthesis in SH-SY5Y cells compared to the glial cell types (Figure 3C). Taken together, these results suggest that subsequent oxidative stress in chronically ER-stressed neuronal cells is partially from eIF2α-mediated translational control while glial cells trigger a sequential acute ISR program. In addition, the inability of ISRIB to fully reverse the effects of chronic stress (Tg 24 h + SA last 0.5 h treatment) in SH-SY5Y cells may be due to eIF2B body composition or localization.

Regulatory remodeling of small eukaryotic initiation factor 2B bodies is specific to the acute phase of the integrated stress response and partially modulated by eIF2α phosphorylation

To investigate the impact of cellular stress on eIF2B localization, we transiently transfected SH-SY5Y, U373, and MO3.13 cells with eIF2Bε-mGFP and treated with the previously described acute (Tg 1h, SA 0.5h) and chronic (Tg 24h, Tg 24h + Tg last 1h, Tg 24h + SA last 0.5h) treatments. We observed an overall increase of eIF2B localization in all cell types although astrocytic cells displayed a higher degree of stimulation (Figure S4). Furthermore, SH-SY5Y and MO3.13 cells showed significantly increased cells harboring localized eIF2B when treated with a VWMD-devised condition (Tg 24h + SA last 0.5h) (Figure S4).

We previously reported increased eIF2Bδ localization to small eIF2B bodies (mainly composed of catalytic γ and ε subunits) upon acute ISR in astrocytes, suggesting the presence of novel eIF2Bγδε subcomplexes.[32] This implies that eIF2Bδ redistribution may play a functional role during cellular ISR, however the specific role is unknown. Given the similarities in the response to acute ISR observed in neuronal and glial cell lines (Figure 3B), we wanted to investigate whether the redistribution of eIF2Bδ was also similarly regulated. We performed immunofluorescence analysis using an eIF2Bδ antibody in SH-SY5Y, U373, and MO3.13 cells expressing eIF2Bε-mGFP (Figure 4Ai). As expected, short-term Tg and SA treatment increased eIF2Bδ localization to small eIF2B bodies in all cell types whilst large eIF2B bodies remained predominantly unchanged (Figure 4Aii). During a chronic ISR treatment (Tg 24h), the eIF2Bδ composition of small bodies returns to control levels (Figure 4Aii) suggesting that this stress-induced eIF2Bδ movement is specific to an acute ISR. Surprisingly, the additional SA treatment after chronic ER stress exposure mirrored the cell type pattern observed for eIF2α phosphorylation (Figure 3Bii). U373 and MO3.13 cells which showed an induction of the acute ISR, also displayed a redistribution of eIF2Bδ to small eIF2B bodies resembling their respective SA-only treatment (Figure 4Aii). In neuronal cells, this acute SA insult after chronic ER stress, which did not induce high levels of eIF2α phosphorylation, failed to significantly enhance eIF2Bδ localization to small eIF2B bodies when compared to levels treated with SA only (Figure 4Aii).

eIF2Bδ redistribution has been previously hypothesized to be modulated by levels of eIF2α-P,[32] and here we further strengthened this hypothesis by observing a mirrored pattern of increased eIF2α-P levels and increased eIF2Bδ to small bodies (Figures 3B and 4A). To investigate whether levels of eIF2α-P influence eIF2Bδ redistribution, we subjected cells to acute Tg treatment in the presence or absence of GSK2606414, a highly selective inhibitor of PERK (PERKi).[44] In line with this, PERKi completely blocked eIF2α phosphorylation and inhibited translation suppression when co-treated with Tg across all cell types (Figure 4Bi). We again performed an immunofluorescence analysis using eIF2Bδ antibody in SH-SY5Y, U373, and MO3.13 cells expressing localized eIF2Bε-mGFP under the previously described Tg and PERKi conditions (Figure 4Bii). Unexpectedly, while we observed a slight increase of eIF2Bδ localization to small bodies in SH-SY5Y and U373 cells when co-treated with Tg and PERKi (thus in the absence of eIF2α phosphorylation), it was significantly lower than when compared to Tg alone treated cells (Figure 4Biii). Moreover, co-treatment of PERKi and Tg treatment exhibited similar levels of eIF2Bδ in small bodies of MO3.13 cells when compared to Tg alone (Figure 4Biii). These data indicate that eIF2Bδ localization to small eIF2B bodies is partially dictated by eIF2α phosphorylation in a cell-type specific manner.

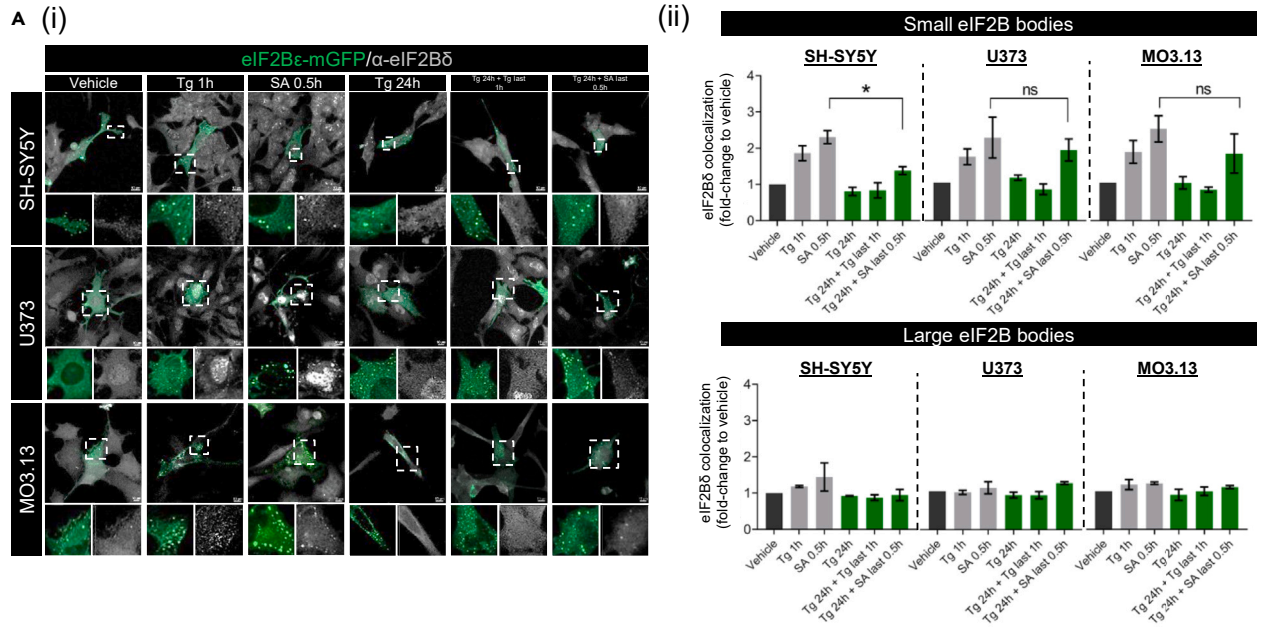
A
(i)
eIF2Bε-mGFP/α-eIF2Bδ
Vehicle
Tg 1h
SA 0.5h
Tg 24h
Tg 24h + Tg last 1h
Tg 24h + SA last 0.5h
SH-SY5Y
U373
MO3.13
(ii)
Small eIF2B bodies
SH-SY5Y
U373
MO3.13
eIF2Bδ colocalization (fold-change to vehicle)
*
ns
ns
Vehicle
Tg 1h
SA 0.5h
Tg 24h
Tg 24h + Tg last 1h
Tg 24h + SA last 0.5h
Large eIF2B bodies
SH-SY5Y
U373
MO3.13
eIF2Bδ colocalization (fold-change to vehicle)

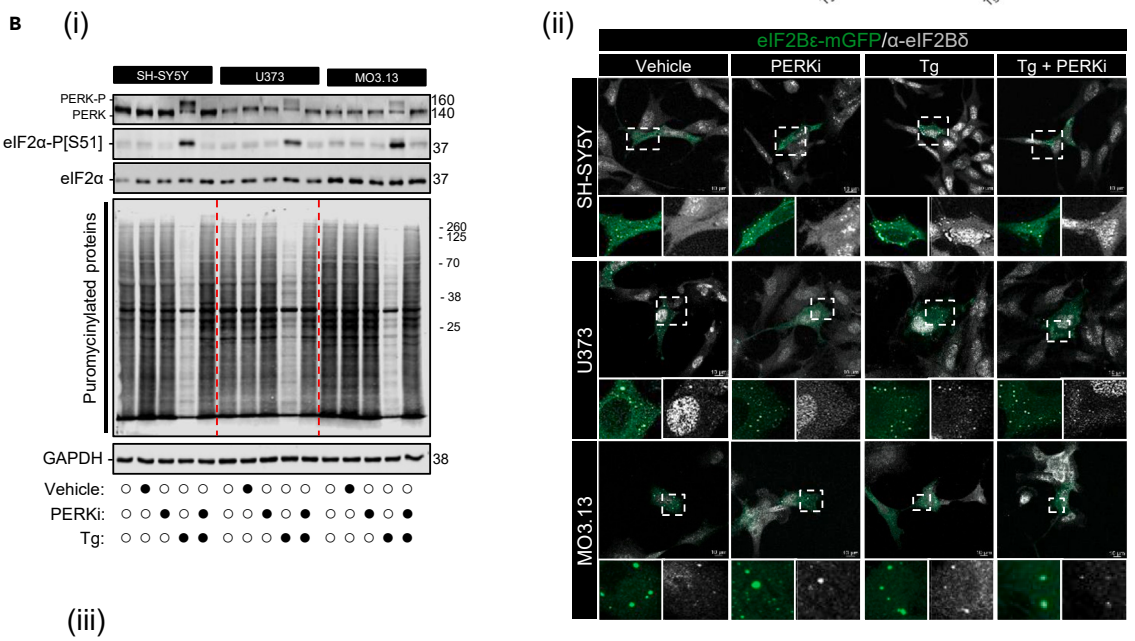
B
(i)
SH-SY5Y
U373
MO3.13
PERK-P
PERK
160
140
eIF2α-P[S51]
37
eIF2α
37
Puromycinylated proteins
260
125
70
38
25
GAPDH
38
Vehicle:
PERKi:
Tg:
(ii)
eIF2Bε-mGFP/α-eIF2Bδ
Vehicle
PERKi
Tg
Tg + PERKi
SH-SY5Y
U373
MO3.13

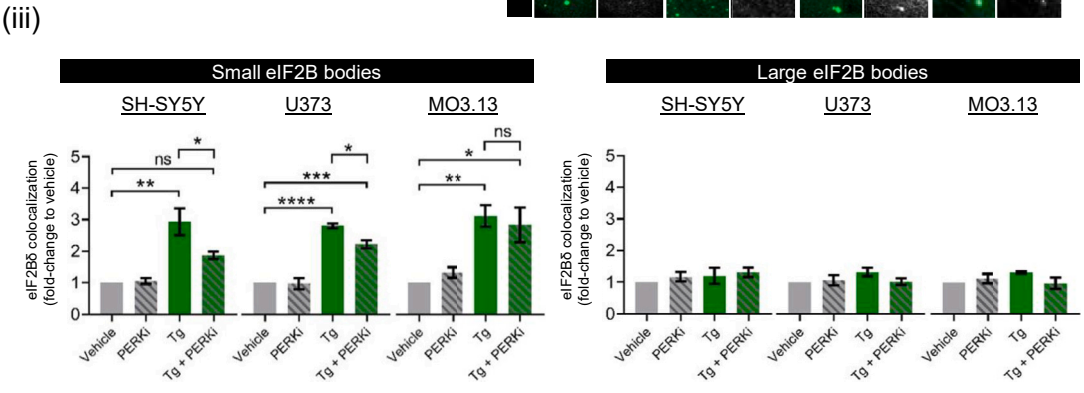
(iii)
Small eIF2B bodies
SH-SY5Y
U373
MO3.13
eIF2Bδ colocalization (fold-change to vehicle)
ns
*
**
***
****
Vehicle
PERKi
Tg
Tg + PERKi
Large eIF2B bodies
SH-SY5Y
U373
MO3.13
eIF2Bδ colocalization (fold-change to vehicle)

Figure 4. eIF2Bδ remodeling of small eIF2B bodies is transient during cellular stress and partially dictated by eIF2α-P[S51] in a cell type dependent manner

(A) (i) Confocal images of SH-SY5Y, U373, and MO3.13 expressing eIF2Bε-mGFP and immunolabelled with anti-eIF2Bδ subjected to acute stress inducers (Tg 1 μM for 1h and SA 125 μM for 30min) or chronic ER stress (Tg 300 nM for 24h) subsequently challenged with previously described acute stress treatments. Scale bar: 10 μm. (ii) Mean percentage of eIF2Bε-mGFP-containing small (*top panel*) and large (*bottom panel*) bodies co-localizing with eIF2Bδ of a population of 30 cells per biological repeat. Fold-change relative to vehicle-treated cells was calculated and analyzed using one-way ANOVA (mean ± SEM; $*p < 0.05$; *ns*, non-significant).

(B) (i) Representative Western blots of the ISR expression profile (PERK-P, PERK, eIF2α-P[S51], pan-eIF2α, CHOP, and GADD34), global newly synthesized proteins (puromycin incorporation assay) and loading control GAPDH in SH-SY5Y, U373 and MO3.13 cells treated with vehicle (DMSO), GSK2606414/PERKi (500 nM), Tg (1μM) or co-treated with PERKi and Tg (PERKi + Tg) for 1h. (ii) Confocal images of SH-SY5Y, U373 and MO3.13 cells expressing eIF2Bε-mGFP and immunolabelled with primary anti-eIF2Bδ subjected to previous treatments. Scale bar: 10 μm. (iii) Mean percentage of eIF2Bε-mGFP-containing small (*left panel*) and large (*right panel*) bodies co-localizing with eIF2Bδ of a population of 30 cells per biological repeat. Fold-change relative to vehicle-treated cells was calculated and analyzed using one-way ANOVA (mean ± SEM; $N = 3$; $*p < 0.05$).

ISRIB's mode of action on eukaryotic initiation factor 2B localization is cell-type specific

ISRIB is an eIF2B activator that attenuates eIF2α-P-dependent translation suppression by promoting decamer formation and enhancing eIF2B GEF activity.[17,18,43] ISRIB does not impact levels of eIF2α phosphorylation *per se* but rather rescues its downstream inhibitory effect on protein synthesis. Previously, we have shown that eIF2Bδ localization to small eIF2B bodies increased as a direct effect of ISRIB's binding to eIF2Bδ.[32] To test whether this is a general cellular feature, we treated SH-SY5Y, U373 and MO3.13 cells expressing eIF2Bε-mGFP with ISRIB (200 nM) for 1h and performed an immunofluorescence analysis using eIF2Bδ antibody (Figure 5Ai). As before, large eIF2B bodies showed no changes in eIF2Bδ composition when exposed to ISRIB alone or in combination with preconditioned Tg treatment for 24h (Figure 5Aii). In contrast, ISRIB treatment showed increased eIF2Bδ localization in small bodies of U373 and MO3.13 cells while a complete absence of eIF2Bδ redistribution was observed in SH-SY5Y cells (Figure 5Aii). Moreover, preconditioning cells to chronic ER stress abrogated eIF2Bδ movement in MO3.13 cells upon ISRIB treatment, whereas it had no impact on U373 cells which showed eIF2Bδ redistribution in all ISRIB conditions (Figure 5Aii). These data provide evidence that ISRIB's mechanism of action may involve cell type specific regulation of eIF2B localization. Given this cell type specific impact of ISRIB in the eIF2B composition of small bodies, we next aimed to investigate if this mirrored a cell-type specific rescue of protein synthesis. Puromycin incorporation assay revealed that adding ISRIB restored protein synthesis in all cell types pre-treated with Tg for 23h (Figures 5Bi and 5ii). Taken together, ISRIB's mode of action is suggested to not be linked to the eIF2Bδ remodeling of small eIF2B bodies in neuronal and oligodendrocytic cells but may be involved in astrocytic cells.

ISRIB and cellular stress selectively modulate the activity of eukaryotic initiation factor 2B bodies in a cell type manner

In addition to the remodeling of eIF2Bδ composition in small eIF2B bodies, we have previously described that both acute stress and ISRIB result in increased shuttling of eIF2 in astrocytic cells.[32] Therefore, we next turned to assess whether there was any cell-specific regulation of eIF2 shuttling in the different cell types upon acute and chronic cellular stress and in the presence or absence of ISRIB treatment. We treated SH-SY5Y, U373, and MO3.13 cells with ISRIB alone or with an acute Tg stress (1h) in the presence or absence of ISRIB and performed FRAP analysis on small and large eIF2B bodies. Intriguingly, cell type disparities were observed in the % recovery of eIF2 in both small and large bodies. For small bodies treated with ISRIB, a significant increase in the % recovery of eIF2 was observed for U373 cells (in line with previously published data) but not for the SH-SY5Y or MO3.13 cells (Figure 6Ai). Upon acute Tg stress, U373 cells displayed an increase in the % recovery of eIF2 into small bodies and this increase was sustained but not increased upon co-treatment with ISRIB (Figure 6Ai). Again, this increase is similar to our previous observations.[32] This increase in recovery of eIF2 in small bodies was unique to U373 cells and was not observed for either the SH-SY5Y or MO3.13 cells (Figure 6Ai). For large eIF2B bodies, ISRIB treatment alone did not impact on eIF2 recovery of any cell lines (Figure 6Aii). However, when cells were treated with acute Tg stress (1h), a decrease in the % recovery of eIF2 was observed for both U373 and SH-SY5Y cells but not for the MO3.13 cells (Figure 6Aii). Furthermore, co-treatment of ISRIB and acute Tg reversed the Tg-induced inhibitory effects on the eIF2 shuttling of large eIF2B bodies in U373 cells, while showing no effect on eIF2B bodies of SH-SY5Y and MO3.13 cells (Figure 6Aii). These data show that acute cellular stress and ISRIB predominantly regulate small and large eIF2B bodies of U373 cells amongst the cell lines used in this study.

We next sought to observe cells with chronic ISR treatment in the presence and absence of ISRIB. In line with the recovery of protein synthesis post-chronic stress, eIF2 recovery was similar to the vehicle control cells post-24h treatment (Figures 6Bi and ii). Moreover, ISRIB treatment in the last hour of the 24h exposure to Tg significantly increased eIF2 recovery of small eIF2B bodies in U373 cells but not in SH-SY5Y or MO3.13 cells (Figure 6Bi), while altogether having no enhancing impact of the activity of large eIF2B bodies (Figure 6Bii). These data suggest that the activity of eIF2B bodies is transiently regulated upon cellular stress and ISRIB modulates small eIF2B bodies during chronic ISR in a cell type manner.

DISCUSSION

We have previously reported that eIF2B bodies represent steady-state autonomous clusters of GEF active eIF2B complexes.[25,29,31,32] Here we show that the prevalence of eIF2B bodies is cell-type specific in unstressed conditions (Figures 1A–1C). Amongst the cell types used in this study, astrocytic cells showed an increased number of cells displaying eIF2B bodies (~54%) in comparison to oligodendrocytic (~33%) and neuronal (~19%) cells. Because localized eIF2B accounts for only a certain portion of total eIF2B, with the remaining GEF exchange occurring

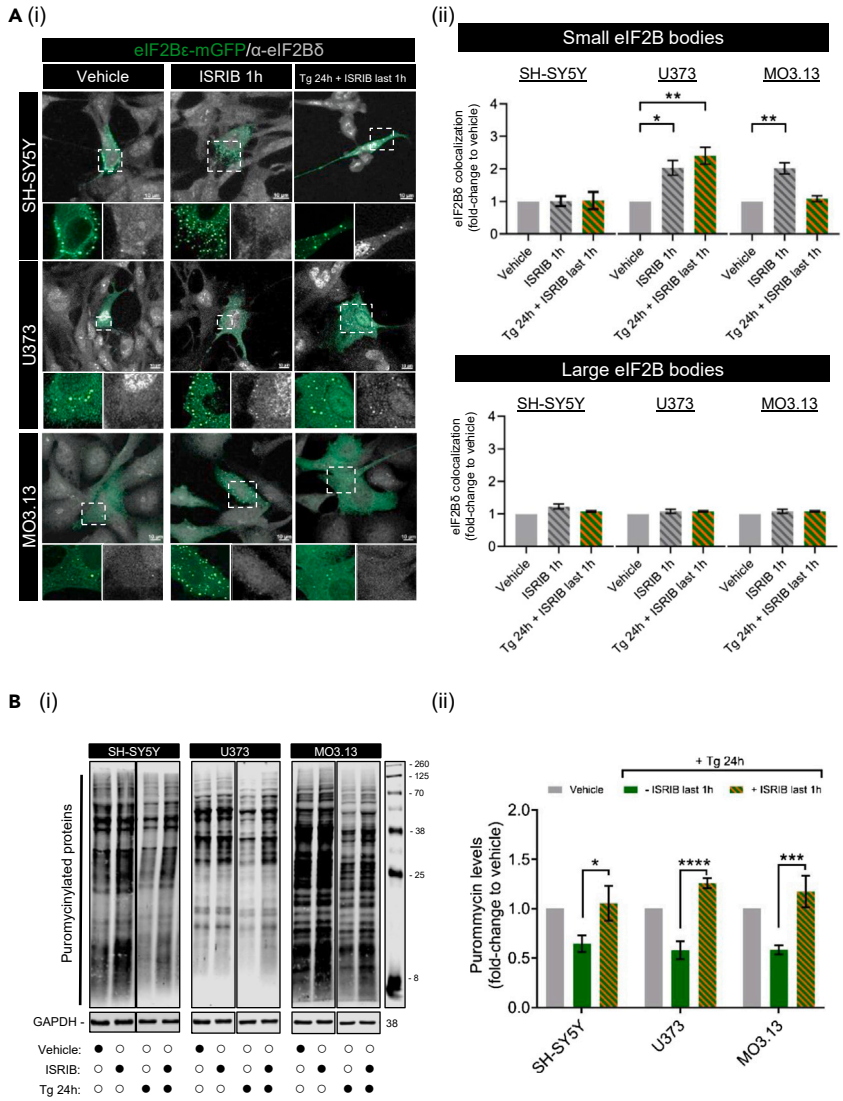

Figure 5. ISRIB restores translation during chronic ER stress while increasing the eIF2Bδ composition of small eIF2B bodies predominantly in astrocytic cells

(A) (i) Confocal images of SH-SY5Y, U373, and MO3.13 expressing eIF2Bε-mGFP and immunolabelled with primary anti-eIF2Bδ subjected to ISRIB (200nM) alone 1h or in combination with preconditioned chronic ER stress treatment (Tg 300nM 24h + ISRIB last 1h). Scale bar: 10 μm. (ii) Mean percentage of eIF2Bε-mGFP-containing small (*top panel*) and large (*bottom panel*) bodies co-localizing with eIF2Bδ. Fold-change relative to vehicle-treated cells was calculated and analyzed using one-way ANOVA (mean ± SEM; $N = 3$; $^{**}p \leq 0.01$, $^{*}p < 0.05$).

(B) (i) Western blotting of global newly synthesized proteins (puromycin incorporation assay) and loading control GAPDH in SH-SY5Y, U373, and MO3.13 cells treated with the same conditions as described previously. (ii) Mean expression levels of puromycin-labeled nascent proteins normalized to housekeeping GAPDH levels. Fold-change relative to vehicle-treated cells was calculated and analyzed using one-way ANOVA (mean ± SEM; $N = 5$–9; $^{****}p \leq 0.001$, $^{***}p \leq 0.001$, $^{*}p < 0.05$).

elsewhere in the cytoplasm, we hypothesize that the degree of eIF2B localization differs depending on the cellular requirement for regulated GEF activity, both for steady state purposes and ability to respond to stress.

A correlation between eIF2B body size and subunit composition was previously reported[32] and now we extend these studies by demonstrating that this correlation is cell-type specific (Figure 1D). Firstly, for the small eIF2B bodies, neuronal cells harbored increased levels of regulatory subunits (eIF2Bα,β,δ) in comparison to both types of glial cells. These data indicate that small eIF2B bodies within astrocytic and oligodendrocytic cells mainly contain eIF2Bγε heterodimers, while in neuronal cells these small bodies contain eIF2B tetrameric and decameric complexes. Secondly, neuronal and astrocytic cells followed the size:subunit relationship as all four subunits (eIF2Bα-γ) showed a higher degree of co-localization to large bodies compared to the small bodies; while oligodendrocytes exhibited the surprising absence of eIF2Bβ and a decreased % of eIF2Bα. These results suggest the full eIF2B decameric complex resides in large eIF2B bodies of neuronal

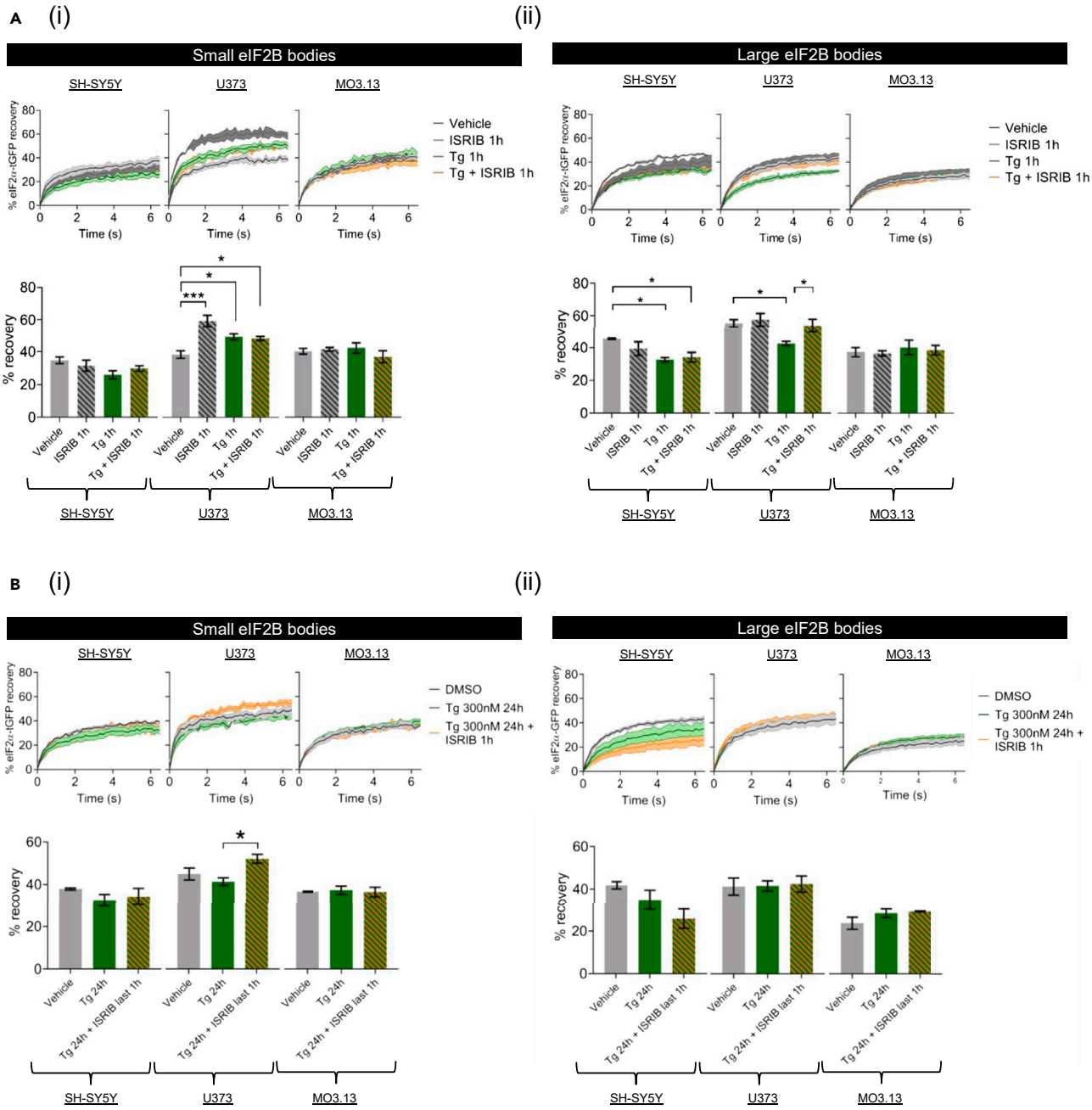

Figure 6. ISRIB modulates the eIF2 shuttling of eIF2B bodies in astrocytic cells

Cells were co-transfected with eIF2α-tGFP to carry out fluorescence recovery after photobleaching (FRAP) analysis, and eIF2Bε-mRFP to locate the eIF2B body. (A) Cells were then treated with vehicle (DMSO), ISRIB (200 nM) alone for 1h, Tg (1 μM) alone for 1h or both treatments in combination (Tg + ISRIB) for 1h. Quantification of normalized FRAP curves for eIF2α-tGFP of at least 10 bodies of small (*right panel*) and large (*left panel*) eIF2Bε-mRFP bodies of SH-SY5Y, U373, and MO3.13 cells. The data were graphed and shown as the mean and S.E.M. bands (*N=3*). The mean percentage of eIF2α-tGFP recovery was determined from normalized FRAP curves (mean ± SEM; $N = 3$; $^{***}p \leq 0.001$, $^{*}p < 0.05$ according to one-way ANOVA).

(B) Cells were then treated with vehicle (DMSO), Tg (300nM) alone for 24h or both treatments in combination where ISRIB was added in the last hour of the 24h period of exposure to Tg. Quantification of normalized FRAP curves for eIF2α-tGFP of at least 10 bodies of small (*right panel*) and large (*left panel*) eIF2Bε-mRFP bodies of SH-SY5Y, U373, and MO3.13 cells. The data were graphed and shown as the mean and S.E.M. bands (*N=3*). Mean percentage of eIF2α-tGFP recovery was determined from normalized FRAP curves (mean ± SEM; $N = 3$; $^{***}p \leq 0.001$, $^{*}p < 0.05$ according to one-way ANOVA).

and astrocytic cells but may not be in oligodendrocytic cells. Given that increased GEF activity of eIF2B correlates with the presence of regulatory eIF2B subunits,[6,13] this decreased association of eIF2Bβ with large eIF2B bodies may account for the decreased basal % eIF2 recovery observed for oligodendrocytes when compared to other cell types (Figure 2B).

eIF2B bodies are targeted during the acute ISR;[32] however, it remains unknown what their significance is upon transition to a chronic ISR. We first aimed to characterize the acute and chronic ISR of neuronal and glial cell lines used in this study. We report that the acute ISR is a general cellular feature as assessed by the canonical eIF2α-dependent pathway of translation shutdown in agreement to a plethora of other cell types.[45–47] Interestingly, we observed a cell-type specific ability to reset an acute-like ISR depending on whether faced with repeated stresses or treated with a different stressor (Figure 3B). In all cells, an initial chronic ER stress was protective toward a second ER stress treatment. This has been shown by others where preconditioning cells to mild eIF2α phosphorylation, either through the inhibition of PP1c or stress-inducing agents,[48] is cytoprotective. Strikingly, replacing the second stress with an oxidative stress elevated eIF2α phosphorylation in glial cells but not in neuronal cells; however, protein synthesis was still targeted in neuronal cells suggesting that this second stress may be regulated via an eIF2α-independent mechanism. Our observations in neuronal cells were strengthened by the fact that ISRIB (which reverses inhibitory effects of eIF2α phosphorylation) was unable to restore translation under these stress conditions (chronic Tg + acute SA) (Figure 3C), but not when treated with Tg alone for 24h in neuronal cells (Figure 5B). Therefore, chronically ER stressed neurons redirect toward an eIF2α-independent mechanism when exposed to oxidative stress. These results are quite unexpected given that GADD34 expression levels are still elevated in these cells (Figure 3B), as GADD34 mRNA levels are known to serve as a molecular memory damper to subsequent stresses.[49–51] This apparent ability of (at least) glial cells to reset the ISR in the presence of GADD34 while neuronal cells seem to "forget" how to respond brings an important question: was it even meant to be remembered? Given this lack of activation of a subsequent ISR in neuronal cells, we consider three possible reasons, but not mutually exclusive, by order of likelihood. (1) The transition to a chronic ISR highlights the inability of neuronal cells to re-shape cell adaptation solely through the ISR, hence shifting toward alternative and/or parallel signaling pathways (e.g., mTOR,[45,52] eIF2A,[53] eIF3d,[42] eEF1A2[54]). Recent evidence supports that translation repression is maintained in PERK-deficient neurons by complementary eIF2α-independent mechanisms (tRNA-cleaving RNase).[55] (2) Secondly, a cell non-autonomous trigger of the acute ISR in neuronal cells undergoing chronic stress signaled by eIF2-dependent glial cells, supported by recent work where targeting the eIF2α-axis of PERK in astrocytes rescues prion-causing neuronal dysfunction.[41] (3) Thirdly, multiple eIF2α kinases might be activated in neuronal cells[55,56] during chronic ER stress, thus less susceptible to restart an acute ISR when subsequently challenged with a different stressor, whereas the glial activation of eIF2α kinases may be stimuli-specific. ISR "exhaustion" has also been recently appreciated where translational-demanding cell types (in this study, pancreatic β cells) are susceptible to ATF4-mediated transcriptome decay when faced with frequent ER stress insults.[57]

Activation of the acute ISR increases eIF2Bδ localization to small eIF2B bodies (containing γ and ε) with increased eIF2 shuttling in astrocytic cells, suggesting the stress-induced formation and clustering of eIF2Bγδε subcomplexes with increased GEF activity.[32] Here we observed that while eIF2Bδ redistributes to small bodies during acute Tg (1h) and SA (0.5h) treatments, it returns to basal levels upon chronic Tg treatment (24h) (Figure 4A); thus, suggesting subunit remodeling of small eIF2B bodies is a transient event and specific to the acute ISR independent of cell types, and reversed during the chronic ISR. Interestingly, a subsequent SA treatment to Tg pre-treated cells, which selectively re-elevates eIF2α phosphorylation in astrocytic and oligodendrocytic cells (Figure 3B), is also accompanied by increased eIF2Bδ localization of small bodies in these cells but not in neuronal cells (Figure 4A). Surprisingly, we show that eIF2Bδ localization to small eIF2B bodies in the presence of acute ER stress is only partially dictated by eIF2α phosphorylation (Figure 4B), suggesting that non-ISR mechanisms are at play in eIF2B body remodeling. We do not discard the possibility that chemical stressors such as Tg may trigger multiple pathways[58,59] that could influence our observations. Given that ER stress-induced eIF2Bδ remodeling exists upon PERK inhibition (yet at a lower level), we speculate that these other pathways could serve as an activator of eIF2B body remodeling, further enhanced and/or maintained by eIF2α phosphorylation.

As shown previously, ISRIB mimicked the acute ISR in astrocytic cells[32] and oligodendrocytic cells; however, chronic ER stress hindered the action of ISRIB for the latter (Figure 5A). However, this "stress-mimicking" feature of ISRIB was not recapitulated in neuronal cells. ISRIB alone or in combination with chronic ER stress did not increase eIF2Bδ localization in neuronal small eIF2B bodies (Figure 5A). Unexpectedly, despite the differences in eIF2Bδ movement, ISRIB treatment of chronic ER-stressed cells had a unanimous restorative effect on translation across all cell types (Figure 5B), thus suggesting that ISRIB-mediated translational rescue does not require increased eIF2Bδ-containing small bodies as a general feature. However, our data suggest that eIF2Bδ regulatory remodeling may be functionally relevant to astrocytic cells.

eIF2B regulatory subunits control eIF2B activity upon stress[10,60] whilst catalytic subunits remain desensitized to stress when uncoupled from regulatory subunits.[13,14] Indeed, FRAP analysis identified a cell-type specific correlation between eIF2B subunit composition and eIF2 recovery upon acute ISR and ISRIB treatment. (1) In neuronal cells, acute ER stress had a predominantly inhibitory effect on the eIF2 recovery of small and large bodies (Figure 6A). This may be a result of a more homogeneous composition of both small and large bodies hence functionally similar. This agrees with our previous observations that neuronal small bodies have increased regulatory subunit composition (Figure 1D). (2) In contrast, astrocytic cells displayed distinctive functional responses for small and large eIF2B bodies as previously reported[32]: small bodies exhibited enhanced eIF2 recovery upon acute ER stress and ISRIB treatment, while acute ER stress repressed the eIF2 recovery of large bodies which is rescued by the addition of ISRIB (Figure 6A). (3) Finally, acute ER stress and ISRIB had no impact on small and large eIF2B bodies of oligodendrocytic cells. This unresponsiveness is likely related to the lack of eIF2Bβ from eIF2B bodies (Figure 1D), hence supporting that non-decameric eIF2B subcomplexes may predominantly localize to eIF2B bodies in oligodendrocytic cells.

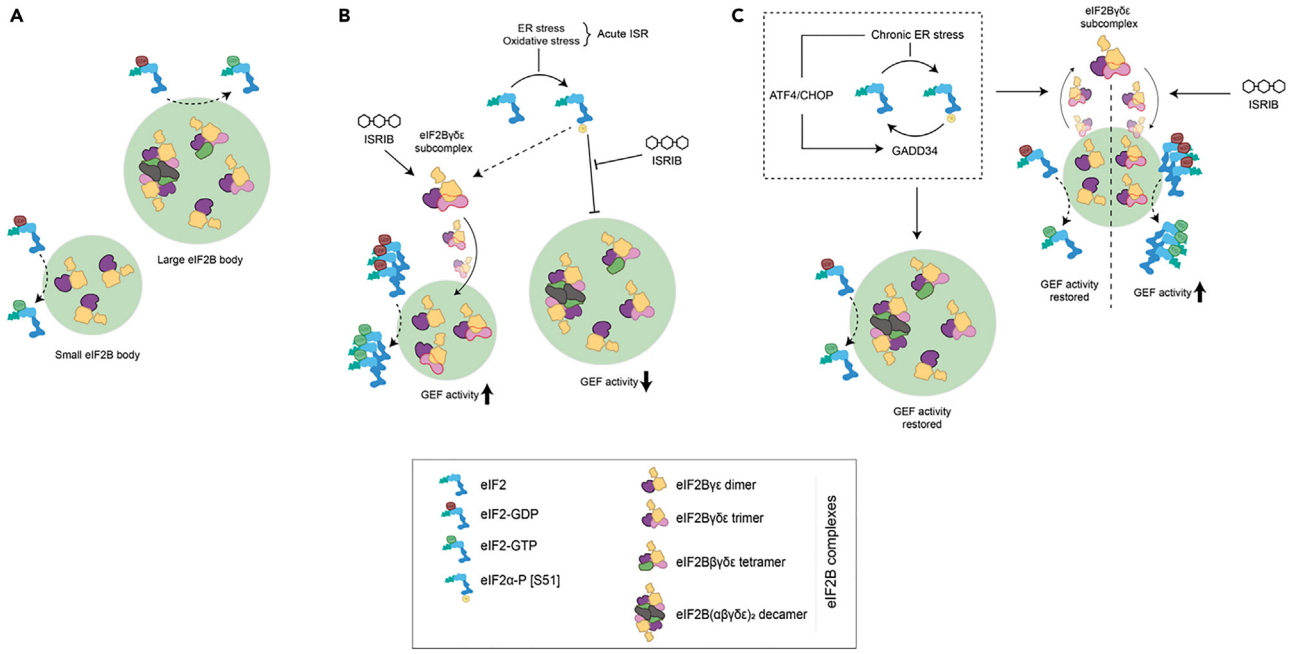

Figure 7. Working model for the impact of cellular stress and ISRIB in eIF2B bodies of astrocytes

(A) eIF2B localizes to small eIF2B bodies containing catalytic subcomplexes and larger eIF2B bodies containing a variety of regulatory subcomplexes (including decameric eIF2B).

(B) Upon the activation of the acute ISR program, eIF2Bγδε subcomplexes are formed and localized to small eIF2B bodies which we hypothesize to have a regulatory role in eIF2B GEF activity; whilst large eIF2B bodies are negatively impacted.

(C) During the transition to a chronic ISR, eIF2Bδ distribution in small bodies is reversed and GEF activity is restored to basal rates, whereas ISRIB treatment bypasses transient eIF2Bδ distribution by prompting extended eIF2Bγδε formation by direct interaction with eIF2Bδ.

While acute ER stress shows cell type dependent discrepancies in the % recovery of eIF2 of eIF2B bodies, these changes are unanimously reversed upon sustained Tg treatment (Figure 6B), further suggesting that eIF2B localization is normalized during chronic ISR. Guan et al. recently provided evidence that recovery of eIF2B activity may not be required upon transition to chronic stress and is alternatively mediated via eIF3.[42]

A cell-specific relationship between eIF2Bδ redistribution and eIF2 recovery was observed in astrocytic cells as illustrated in Figure 7. Indeed, ISRIB treatment has a dominant effect of increasing the eIF2δ composition of small bodies, either alone or in combination with chronic ER stress (Figure 5A), accompanied by enhanced % recovery of eIF2 (Figure 6B). This relationship is not recapitulated in the other cell types used in this study, which requires further *in vitro* studies to investigate the cell specific GEF activity of eIF2Bγδε subcomplexes.

Collectively, our results demonstrate that cells display cell type specific localization and regulation of eIF2B bodies. The existence of different eIF2B subcomplexes of eIF2B bodies may allow unique rates of ternary complexes levels and adaptability to stress which overall might make translation more efficient and/or more easily regulated. More importantly, we provide evidence for cell-type specific fine-tuning of eIF2B function and regulation, the core event of the ISR; further emphasizing the need to tailor therapeutic interventions in a cell type manner.

Limitations of the study

The study was performed in generic cancer-derived cell lines and does not recapitulate the metabolic burden of non-cancerous neurons and astrocytes[61] which might skew the observations reported here on the magnitude activity of the ISR and stress-induced effect on eIF2B bodies given the intimate link between cancer and the ISR.[62] In fact, primary human astrocytes have overall higher levels of eIF2α-P upon cellular stress although translation inhibition is like U373 cells (data not shown). Furthermore, SH-SY5Y, despite being a dopaminergic neural cell line, is cell-dividing and is not representative of a post-mitotic neuronal model. To surpass these issues, future work should be conducted in iPSC-derived neural progenitor cells (NPCs) differentiated into neurons, astrocytes, and oligodendrocytes.[63] Perhaps, even more importantly, is establishing a co-cultured system to confirm the findings reported in this study and offer clinical relevance to VWMD therapy. The experimental setup of this study aimed to explore the individual contribution of cell types in eIF2B localization and stress response profiles; however, the cell-to-cell crosstalk is crucial for proper neuronal metabolism (e.g., lactate deliverance from astrocytes), synaptic trafficking and are central of VWMD's cell-specific vulnerability.[38] A 3D organoid with VWMD patient-derived iPSCs has been recently developed and fully recapitulates VWMD's main pathological hallmarks (GFAPδ expression, immature oligodendrocytes, sparse myelin),[64] while cultured

astrocytes from VWMD mutant eIF2Bε(R191H) mice lose *in vivo* diseased phenotype (hypersensitive ISR) and instead behave like healthy astrocytes[65]; altogether showing that future studies should devise co-cultured platforms to investigate ISR regulation and VWMD pathomechanisms.

RESOURCE AVAILABILITY

Lead contact

Further information and requests for reagents should be directed to and will be fulfilled by the lead contact: Susan Campbell (susan.campbell@shu.ac.uk), Biomolecular Science Research Center, Sheffield Hallam University, City Campus, Howard Street, S1 1WB, Sheffield, United Kingdom.

Materials availability

All materials generated in this study are available from the lead contact upon request.

Data and code availability

- Original immunoblots have been deposited at Mendeley Data Repository and are publicly available. The DOI is https://doi.org/10.17632/tjtcftj3cf.1. Microscopy data reported in this article will be shared by the lead contact upon request.
- This article does not report original code.
- Any additional information required to reanalyze the data reported in this article is available from the lead contact upon request.

ACKNOWLEDGMENTS

The authors wish to thank Dr Truus Abbink (Amsterdam UMC) for insightful discussions and helpful suggestions. We thank Professor Nicola Woodroofe (Sheffield Hallam University) for kindly gifting us the MO3.13 cells and selective marker antibodies. We gratefully thank the Biomolecular Sciences Research Center and Sheffield Hallam University for funding this work. Graphical abstract created with BioRender.com.

AUTHOR CONTRIBUTIONS

F.M.H. and M.I.R.d.O., performed experiments; F.M.H., M.I.R.d.O, A.K.C., K.E.A., and S.G.C. analyzed data and assisted with experimental design; A.K.C., K.E.A., and S.G.C., project supervision. F.M.H., S.G.C., wrote the article with assistance from other authors. All authors have reviewed and approved the final article.

DECLARATION OF INTERESTS

The authors have no relevant financial or non-financial interests to disclose.

The author Dr Filipe Hanson completed this work as part of his PhD studies at Sheffield Hallam University. He now works as a Research Scientist for UCB Pharma, Slough, UK. The author Dr Madalena deOliveira contributed to this work as part of her PhD studies at Sheffield Hallam University. She now works as a Postdoctoral Fellow for MSD, UK.

STAR★METHODS

Detailed methods are provided in the online version of this paper and include the following:

- KEY RESOURCES TABLE
- EXPERIMENTAL MODEL AND STUDY PARTICIPANT DETAILS
- METHOD DETAILS
  - Cell treatments
  - Plasmids
  - Transient transfection procedures
  - Immunoblotting
  - Puromycin incorporation assay
  - Immunocytochemistry
  - Confocal imaging and fluorescence recovery after photo bleaching (FRAP)
- QUANTIFICATION AND STATISTICAL ANALYSIS

SUPPLEMENTAL INFORMATION

Supplemental information can be found online at https://doi.org/10.1016/j.isci.2024.110851.

Received: January 16, 2024
Revised: April 30, 2024
Accepted: August 27, 2024
Published: August 30, 2024

REFERENCES

1. Naveau, M., Lazennec-Schurdevin, C., Panvert, M., Dubiez, E., Mechulam, Y., and Schmitt, E. (2013). Roles of yeast eIF2alpha and eIF2beta subunits in the binding of the initiator methionyl-tRNA. Nucleic Acids Res. *41*, 1047–1057. https://doi.org/10.1093/nar/gks1180.
2. Schmitt, E., Panvert, M., Lazennec-Schurdevin, C., Coureux, P.D., Perez, J., Thompson, A., and Mechulam, Y. (2012). Structure of the ternary initiation complex aIF2-GDPNP-methionylated initiator tRNA. Nat. Struct. Mol. Biol. *19*, 450–454. https://doi.org/10.1038/nsmb.2259.
3. Hinnebusch, A.G., and Lorsch, J.R. (2012). The mechanism of eukaryotic translation initiation: new insights and challenges. Cold Spring Harbor Perspect. Biol. *4*, a011544. https://doi.org/10.1101/cshperspect.a011544.
4. Paulin, F.E., Campbell, L.E., O'Brien, K., Loughlin, J., and Proud, C.G. (2001). Eukaryotic translation initiation factor 5 (eIF5) acts as a classical GTPase-activator protein. Curr. Biol. *11*, 55–59. https://doi.org/10.1016/s0960-9822(00)00025-7.
5. Jennings, M.D., Zhou, Y., Mohammad-Qureshi, S.S., Bennett, D., and Pavitt, G.D. (2013). eIF2B promotes eIF5 dissociation from eIF2*GDP to facilitate guanine nucleotide exchange for translation initiation. Genes Dev. *27*, 2696–2707. https://doi.org/10.1101/gad.231514.113.
6. Williams, D.D., Pavitt, G.D., and Proud, C.G. (2001). Characterization of the initiation factor eIF2B and its regulation in Drosophila melanogaster. J. Biol. Chem. *276*, 3733–3742. https://doi.org/10.1074/jbc.M008041200.
7. Bogorad, A.M., Xia, B., Sandor, D.G., Mamonov, A.B., Cafarella, T.R., Jehle, S., Vajda, S., Kozakov, D., and Marintchev, A. (2014). Insights into the architecture of the eIF2Balpha/beta/delta regulatory subcomplex. Biochemistry *53*, 3432–3445. https://doi.org/10.1021/bi500346u.
8. Kimball, S.R., Horetsky, R.L., and Jefferson, L.S. (1998). Implication of eIF2B rather than eIF4E in the regulation of global protein synthesis by amino acids in L6 myoblasts. J. Biol. Chem. *273*, 30945–30953. https://doi.org/10.1074/jbc.273.47.30945.
9. Pavitt, G.D., Ramaiah, K.V., Kimball, S.R., and Hinnebusch, A.G. (1998). eIF2 independently binds two distinct eIF2B subcomplexes that catalyze and regulate guanine-nucleotide exchange. Genes Dev. *12*, 514–526. https://doi.org/10.1101/gad.12.4.514.
10. Pavitt, G.D., Yang, W., and Hinnebusch, A.G. (1997). Homologous segments in three subunits of the guanine nucleotide exchange factor eIF2B mediate translational regulation by phosphorylation of eIF2. Mol. Cell Biol. *17*, 1298–1313. https://doi.org/10.1128/mcb.17.3.1298.
11. Tsai, J.C., Miller-Vedam, L.E., Anand, A.A., Jaishankar, P., Nguyen, H.C., Renslo, A.R., Frost, A., and Walter, P. (2018). Structure of the nucleotide exchange factor eIF2B reveals mechanism of memory-enhancing molecule. Science (New York, N.Y.) *359*, eaaq0939. https://doi.org/10.1126/science.aaq0939.
12. Zyryanova, A.F., Weis, F., Faille, A., Alard, A.A., Crespillo-Casado, A., Sekine, Y., Harding, H.P., Allen, F., Parts, L., Fromont, C., et al. (2018). Binding of ISRIB reveals a regulatory site in the nucleotide exchange factor eIF2B. Science (New York, N.Y.) *359*, 1533–1536. https://doi.org/10.1126/science.aar5129.
13. Liu, R., van der Lei, H.D.W., Wang, X., Wortham, N.C., Tang, H., van Berkel, C.G.M., Mufunde, T.A., Huang, W., van der Knaap, M.S., Scheper, G.C., and Proud, C.G. (2011). Severity of vanishing white matter disease does not correlate with deficits in eIF2B activity or the integrity of eIF2B complexes. Hum. Mutat. *32*, 1036–1045. https://doi.org/10.1002/humu.21535.
14. Wortham, N.C., Martinez, M., Gordiyenko, Y., Robinson, C.V., and Proud, C.G. (2014). Analysis of the subunit organization of the eIF2B complex reveals new insights into its structure and regulation. FASEB (Fed. Am. Soc. Exp. Biol.) J. *28*, 2225–2237. https://doi.org/10.1096/fj.13-243329.
15. Pakos-Zebrucka, K., Koryga, I., Mnich, K., Ljujic, M., Samali, A., and Gorman, A.M. (2016). The integrated stress response. EMBO Rep. *17*, 1374–1395.
16. Hanson, F.M., Hodgson, R.E., de Oliveira, M.I.R., Allen, K.E., and Campbell, S.G. (2022). Regulation and function of eIF2B in neurological and metabolic disorders. Biosci. Rep. *42*, BSR20211699. https://doi.org/10.1042/BSR20211699.
17. Schoof, M., Boone, M., Wang, L., Lawrence, R., Frost, A., and Walter, P. (2021). eIF2B conformation and assembly state regulate the integrated stress response. Elife *10*, e65703. https://doi.org/10.7554/eLife.65703.
18. Zyryanova, A.F., Kashiwagi, K., Rato, C., Harding, H.P., Crespillo-Casado, A., Perera, L.A., Sakamoto, A., Nishimoto, M., Yonemochi, M., Shirouzu, M., et al. (2021). ISRIB Blunts the Integrated Stress Response by Allosterically Antagonising the Inhibitory Effect of Phosphorylated eIF2 on eIF2B. Mol. Cell *81*, 88–103.e6. https://doi.org/10.1016/j.molcel.2020.10.031.
19. Adomavicius, T., Guaita, M., Zhou, Y., Jennings, M.D., Latif, Z., Roseman, A.M., and Pavitt, G.D. (2019). The structural basis of translational control by eIF2 phosphorylation. Nat. Commun. *10*, 2136. https://doi.org/10.1038/s41467-019-10167-3.
20. Kashiwagi, K., Ito, T., and Yokoyama, S. (2017). Crystal structure of eIF2B and insights into eIF2-eIF2B interactions. FEBS J. *284*, 868–874. https://doi.org/10.1111/febs.13896.
21. Kashiwagi, K., Yokoyama, T., Nishimoto, M., Takahashi, M., Sakamoto, A., Yonemochi, M., Shirouzu, M., and Ito, T. (2019). Structural basis for eIF2B inhibition in integrated stress response. Science (New York, N.Y.) *364*, 495–499. https://doi.org/10.1126/science.aaw4104.
22. Kashiwagi, K., Takahashi, M., Nishimoto, M., Hiyama, T.B., Higo, T., Umehara, T., Sakamoto, K., Ito, T., and Yokoyama, S. (2016). Crystal structure of eukaryotic translation initiation factor 2B. Nature *531*, 122–125. https://doi.org/10.1038/nature16991.
23. Harding, H.P., Novoa, I., Zhang, Y., Zeng, H., Wek, R., Schapira, M., and Ron, D. (2000). Regulated translation initiation controls stress-induced gene expression in mammalian cells. Mol. Cell *6*, 1099–1108.
24. Bond, S., Lopez-Lloreda, C., Gannon, P.J., Akay-Espinoza, C., and Jordan-Sciutto, K.L. (2020). The Integrated Stress Response and Phosphorylated Eukaryotic Initiation Factor 2α in Neurodegeneration. J. Neuropathol. Exp. Neurol. *79*, 123–143. https://doi.org/10.1093/jnen/nlz129.
25. Campbell, S.G., Hoyle, N.P., and Ashe, M.P. (2005). Dynamic cycling of eIF2 through a large eIF2B-containing cytoplasmic body: implications for translation control. J. Cell Biol. *170*, 925–934.
26. Campbell, S.G., and Ashe, M.P. (2006). Localization of the translational guanine nucleotide exchange factor eIF2B: a common theme for GEFs? Cell Cycle *5*, 678–680. https://doi.org/10.4161/cc.5.7.2607.
27. Egbe, N.E., Paget, C.M., Wang, H., and Ashe, M.P. (2015). Alcohols inhibit translation to regulate morphogenesis in C. albicans. Fungal Genet. Biol. *77*, 50–60. https://doi.org/10.1016/j.fgb.2015.03.008.
28. Moon, S.L., and Parker, R. (2018). Analysis of eIF2B bodies and their relationships with stress granules and P-bodies. Sci. Rep. *8*, 12264. https://doi.org/10.1038/s41598-018-30805-y.
29. Norris, K., Hodgson, R.E., Dornelles, T., Allen, K.E., Abell, B.M., Ashe, M.P., and Campbell, S.G. (2021). Mutational analysis of the alpha subunit of eIF2B provides insights into the role of eIF2B bodies in translational control and VWM disease. J. Biol. Chem. *296*, 100207. https://doi.org/10.1074/jbc.RA120.014956.
30. Nüske, E., Marini, G., Richter, D., Leng, W., Bogdanova, A., Franzmann, T.M., Pigino, G., and Alberti, S. (2020). Filament formation by the translation factor eIF2B regulates protein synthesis in starved cells. Biology Open *9*, bio046391. https://doi.org/10.1242/bio.046391.
31. Taylor, E.J., Campbell, S.G., Griffiths, C.D., Reid, P.J., Slaven, J.W., Harrison, R.J., Sims, P.F.G., Pavitt, G.D., Delneri, D., and Ashe, M.P. (2010). Fusel alcohols regulate translation initiation by inhibiting eIF2B to reduce ternary complex in a mechanism that may involve altering the integrity and dynamics of the eIF2B body. Mol. Biol. Cell *21*, 2202–2216. https://doi.org/10.1091/mbc.E09-11-0962.
32. Hodgson, R.E., Varanda, B.A., Ashe, M.P., Allen, K.E., and Campbell, S.G. (2019). Cellular eIF2B subunit localization: implications for the integrated stress response and its control by small molecule drugs. Mol. Biol. Cell *30*, 942–958. https://doi.org/10.1091/mbc.E18-08-0538.
33. van der Knaap, M.S., Pronk, J.C., and Scheper, G.C. (2006). Vanishing white matter disease. Lancet Neurol. *5*, 413–423.
34. Bugiani, M., Boor, I., van Kollenburg, B., Postma, N., Polder, E., van Berkel, C., van Kesteren, R.E., Windrem, M.S., Hol, E.M., Scheper, G.C., et al. (2011). Defective glial maturation in vanishing white matter disease. J. Neuropathol. Exp. Neurol. *70*, 69–82. https://doi.org/10.1097/NEN.0b013e318203ae74.
35. Dooves, S., Bugiani, M., Postma, N.L., Polder, E., Land, N., Horan, S.T., van Deijk, A.L.F., van de Kreeke, A., Jacobs, G., Vuong, C., et al. (2016). Astrocytes are central in the pathomechanisms of vanishing white matter. J. Clin. Invest. *126*, 1512–1524. https://doi.org/10.1172/JCI83908.
36. Dooves, S., Bugiani, M., Wisse, L.E., Abbink, T.E.M., van der Knaap, M.S., and Heine, V.M. (2018). Bergmann glia translocation: a new disease marker for vanishing white matter identifies therapeutic effects of Guanabenz

treatment. Neuropathol. Appl. Neurobiol. *44*, 391–403. https://doi.org/10.1111/nan.12411.

37. Herrero, M., Mandelboum, S., and Elroy-Stein, O. (2019). eIF2B Mutations Cause Mitochondrial Malfunction in Oligodendrocytes. NeuroMolecular Med. *21*, 303–313. https://doi.org/10.1007/s12017-019-08551-9.
38. Klok, M.D., Bugiani, M., de Vries, S.I., Gerritsen, W., Breur, M., van der Sluis, S., Heine, V.M., Kole, M.H.P., Baron, W., and van der Knaap, M.S. (2018). Axonal Abnormalities in Vanishing White Matter (Wiley Periodicals, Inc on behalf of American Neurological Association). https://doi.org/10.1002/acn3.540.
39. Leferink, P.S., Breeuwsma, N., Bugiani, M., van der Knaap, M.S., and Heine, V.M. (2018). Affected astrocytes in the spinal cord of the leukodystrophy vanishing white matter. Glia *66*, 862–873. https://doi.org/10.1002/glia.23289.
40. Gomez, E., and Pavitt, G.D. (2000). Identification of domains and residues within the epsilon subunit of eukaryotic translation initiation factor 2B (eIF2Bepsilon) required for guanine nucleotide exchange reveals a novel activation function promoted by eIF2B complex formation. Mol. Cell Biol. *20*, 3965–3976. https://doi.org/10.1128/MCB.20.11.3965-3976.2000.
41. Smith, H.L., Freeman, O.J., Butcher, A.J., Holmqvist, S., Humoud, I., Schätzl, T., Hughes, D.T., Verity, N.C., Swinden, D.P., Hayes, J., et al. (2020). Astrocyte Unfolded Protein Response Induces a Specific Reactivity State that Causes Non-Cell-Autonomous Neuronal Degeneration. Neuron *105*, 855–866.e5.
42. Guan, B.J., van Hoef, V., Jobava, R., Elroy-Stein, O., Valasek, L.S., Cargnello, M., Gao, X.H., Krokowski, D., Merrick, W.C., Kimball, S.R., et al. (2017). A Unique ISR Program Determines Cellular Responses to Chronic Stress. Mol. Cell *68*, 885–900.e6.
43. Sidrauski, C., Acosta-Alvear, D., Khoutorsky, A., Vedantham, P., Hearn, B.R., Li, H., Gamache, K., Gallagher, C.M., Ang, K.K.H., Wilson, C., et al. (2013). Pharmacological brake-release of mRNA translation enhances cognitive memory. Elife *2*, e00498. https://doi.org/10.7554/eLife.00498.
44. Halliday, M., Hughes, D., and Mallucci, G.R. (2017). Fine-tuning PERK signaling for neuroprotection. J. Neurochem. *142*, 812–826. https://doi.org/10.1111/jnc.14112.
45. Guan, B.J., Krokowski, D., Majumder, M., Schmotzer, C.L., Kimball, S.R., Merrick, W.C., Koromilas, A.E., and Hatzoglou, M. (2014). Translational control during endoplasmic reticulum stress beyond phosphorylation of the translation initiation factor eIF2α. J. Biol. Chem. *289*, 12593–12611. https://doi.org/10.1074/jbc.M113.543215.
46. Spaan, C.N., Smit, W.L., van Lidth de Jeude, J.F., Meijer, B.J., Muncan, V., van den Brink, G.R., and Heijmans, J. (2019). Expression of UPR effector proteins ATF6 and XBP1 reduce colorectal cancer cell proliferation and stemness by activating PERK signaling. Cell Death Dis. *10*, 490. https://doi.org/10.1038/s41419-019-1729-4.
47. Teske, B.F., Wek, S.A., Bunpo, P., Cundiff, J.K., McClintick, J.N., Anthony, T.G., and Wek, R.C. (2011). The eIF2 kinase PERK and the integrated stress response facilitate activation of ATF6 during endoplasmic reticulum stress. Mol. Biol. Cell *22*, 4390–4405. https://doi.org/10.1091/mbc.E11-06-0510.
48. Lu, P.D., Jousse, C., Marciniak, S.J., Zhang, Y., Novoa, I., Scheuner, D., Kaufman, R.J., Ron, D., and Harding, H.P. (2004). Cytoprotection by pre-emptive conditional phosphorylation of translation initiation factor 2. EMBO J. *23*, 169–179. https://doi.org/10.1038/sj.emboj.7600030.
49. Batjargal, T., Zappa, F., Grant, R.J., Piscopio, R.A., Chialastri, A., Dey, S.S., Acosta-Alvear, D., and Wilson, M.Z. (2022). Optogenetic control of the integrated stress response reveals proportional encoding and the stress memory landscape. Preprint at bioRxiv. https://doi.org/10.1101/2022.05.24.493309.
50. Klein, P., Kallenberger, S.M., Roth, H., Roth, K., Ly-Hartig, T.B.N., Magg, V., Aleš, J., Talemi, S.R., Qiang, Y., Wolf, S., et al. (2022). Temporal control of the integrated stress response by a stochastic molecular switch. Sci. Adv. *8*, eabk2022. https://doi.org/10.1126/sciadv.abk2022.
51. Shelkovnikova, T.A., Dimasi, P., Kukharsky, M.S., An, H., Quintiero, A., Schirmer, C., Buée, L., Galas, M.C., and Buchman, V.L. (2017). Chronically stressed or stress-preconditioned neurons fail to maintain stress granule assembly. Cell Death Dis. *8*, e2788. https://doi.org/10.1038/cddis.2017.199.
52. Terenzio, M., Koley, S., Samra, N., Rishal, I., Zhao, Q., Sahoo, P.K., Urisman, A., Marvaldi, L., Oses-Prieto, J.A., Forester, C., et al. (2018). Locally translated mTOR controls axonal local translation in nerve injury. Science (New York, N.Y.) *359*, 1416–1421. https://doi.org/10.1126/science.aan1053.
53. Kim, J.H., Park, S.M., Park, J.H., Keum, S.J., and Jang, S.K. (2011). eIF2A mediates translation of hepatitis C viral mRNA under stress conditions. EMBO J. *30*, 2454–2464. https://doi.org/10.1038/emboj.2011.146.
54. Mendoza, M.B., Gutierrez, S., Ortiz, R., Moreno, D.F., Dermit, M., Dodel, M., Rebollo, E., Bosch, M., Mardakheh, F.K., and Gallego, C. (2021). The elongation factor eEF1A2 controls translation and actin dynamics in dendritic spines. Sci. Signal. *14*, eabf5594. https://doi.org/10.1126/scisignal.abf5594.
55. Wolzak, K., Nölle, A., Farina, M., Abbink, T.E., van der Knaap, M.S., Verhage, M., and Scheper, W. (2022). Neuron-specific translational control shift ensures proteostatic resilience during ER stress. EMBO J. *41*, e110501. https://doi.org/10.15252/embj.2021110501.
56. Alvarez-Castelao, B., Tom Dieck, S., Fusco, C.M., Donlin-Asp, P., Perez, J.D., and Schuman, E.M. (2020). The switch-like expression of heme-regulated kinase 1 mediates neuronal proteostasis following proteasome inhibition. Elife *9*, e52714. https://doi.org/10.7554/eLife.52714.
57. Chen, C.W., Guan, B.J., Alzahrani, M.R., Gao, Z., Gao, L., Bracey, S., Wu, J., Mbow, C.A., Jobava, R., Haataja, L., et al. (2022). Adaptation to chronic ER stress enforces pancreatic β-cell plasticity. Nat. Commun. *13*, 4621. https://doi.org/10.1038/s41467-022-32425-7.
58. Li, L., and Hu, G.K. (2015). Pink1 protects cortical neurons from thapsigargin-induced oxidative stress and neuronal apoptosis. Biosci. Rep. *35*, e00174. https://doi.org/10.1042/BSR20140104.
59. Wink, S., Hiemstra, S., Herpers, B., and van de Water, B. (2017). High-content imaging-based BAC-GFP toxicity pathway reporters to assess chemical adversity liabilities. Arch. Toxicol. *91*, 1367–1383. https://doi.org/10.1007/s00204-016-1781-0.
60. Krishnamoorthy, T., Pavitt, G.D., Zhang, F., Dever, T.E., and Hinnebusch, A.G. (2001). Tight binding of the phosphorylated alpha subunit of initiation factor 2 (eIF2alpha) to the regulatory subunits of guanine nucleotide exchange factor eIF2B is required for inhibition of translation initiation. Mol. Cell Biol. *21*, 5018–5030. https://doi.org/10.1128/MCB.21.15.5018-5030.2001.
61. Ikari, R., Mukaisho, K.I., Kageyama, S., Nagasawa, M., Kubota, S., Nakayama, T., Murakami, S., Taniura, N., Tanaka, H., Kushima, R.P., and Kawauchi, A. (2021). Differences in the Central Energy Metabolism of Cancer Cells between Conventional 2D and Novel 3D Culture Systems. Int. J. Mol. Sci. *22*, 1805. https://doi.org/10.3390/ijms22041805.
62. Licari, E., Sánchez-Del-Campo, L., and Falletta, P. (2021). The two faces of the Integrated Stress Response in cancer progression and therapeutic strategies. Int. J. Biochem. Cell Biol. *139*, 106059. https://doi.org/10.1016/j.biocel.2021.106059.
63. Ladran, I., Tran, N., Topol, A., and Brennand, K.J. (2013). Neural stem and progenitor cells in health and disease. Wiley Interdiscip. Rev. Syst. Biol. Med. *5*, 701–715. https://doi.org/10.1002/wsbm.1239.
64. Deng, J., Zhang, J., Gao, K., Zhou, L., Jiang, Y., Wang, J., and Wu, Y. (2023). Human-induced pluripotent stem cell-derived cerebral organoid of leukoencephalopathy with vanishing white matter. CNS Neurosci. Ther. *29*, 1049–1066. https://doi.org/10.1111/cns.14079.
65. Wisse, L.E., Ter Braak, T.J., van de Beek, M.C., van Berkel, C.G.M., Wortel, J., Heine, V.M., Proud, C.G., van der Knaap, M.S., and Abbink, T.E.M. (2018). Adult mouse eIF2Bε Arg191His astrocytes display a normal integrated stress response *in vitro*. Sci. Rep. *8*, 3773. https://doi.org/10.1038/s41598-018-21885-x.

STAR★METHODS

KEY RESOURCES TABLE

REAGENT or RESOURCE	SOURCE	IDENTIFIER
Antibodies		
Rabbit polyclonal anti-eIF2Bα	Proteintech	Cat# 18010-1-AP; RRID: AB_2261996
Rabbit polyclonal anti-eIF2Bβ	Proteintech	Cat# 11034-1-AP; RRID: AB_2096016
Mouse monoclonal anti-eIF2Bγ	Santa Cruz Biotechnology	Cat# sc-137248; RRID: AB_2096150
Mouse monoclonal anti-eIF2Bδ	Santa Cruz Biotechnology	Cat# sc-271332; RRID: AB_10610502
Rabbit polyclonal anti-eIF2Bε	Sigma-Aldrich	Cat# HPA069303; RRID: AB_2686114
Mouse monoclonal anti-eIF2α	Abcam	Cat# ab5369; RRID: AB_304838
Rabbit recombinant monoclonal anti-eIF2α[ser51-P] [E90]	Abcam	Cat# ab32157; RRID: AB_732117
Rabbit polyclonal anti-PERK	Proteintech	Cat# 20582-1-AP; RRID: AB_10695760
Rabbit polyclonal anti-GADD34	Proteintech	Cat# 10449-1-AP; RRID: AB_2168724
Rabbit polyclonal anti-CHOP	Proteintech	Cat# 15204-1-AP; RRID: AB_2292610
Rabbit monoclonal anti-ATF4 (discontinued)	Abcam	Cat# ab184909; RRID: AB_2819059
Rabbit monoclonal anti-GAPDH	Cell Signaling Technology	Cat# 2118; RRID: AB_10693448
Mouse monoclonal anti-puromycin (clone 12D10)	Merck Millipore	Cat# MABE343; RRID: AB_2566826
Mouse anti-GFAP	This work	N/A
Rabbit polyclonal anti-MBP	Abcam	Cat# ab40390; RRID: AB_1141521
Mouse monoclonal anti-NeuN	Abcam	Cat# ab104224; RRID: AB_10711040
Goat anti-rabbit IRDye 680RD	LI-COR	Cat# 925–68071; RRID: AB_2721181
Goat anti-mouse IRDye 800CW	LI-COR	Cat# 925–32210; RRID: AB_2687825
Goat anti-Rabbit Alexa Fluor 594®	Invitrogen	Cat# A-11012; RRID: AB_2534079
Goat anti-Mouse Alexa Fluor 594®	Invitrogen	Cat# A-11032; RRID: AB_2534091
Goat anti-Mouse Alexa Fluor 488®	Invitrogen	Cat# A-11001; RRID: AB_2534069
Goat anti-Rabbit Alexa Fluor 488®	Invitrogen	Cat# A-11008; RRID: AB_143165
Chemicals, peptides, and recombinant proteins		
Thapsigargin (Tg)	Sigma-Aldrich	Cat# T9033
Sodium arsenite (SA)	Sigma-Aldrich	Cat# S7400
Tunicamycin (Tm)	Cayman Chemical	Cat# 11445
GSK2606414 (PERK inhibitor)	Tocris	Cat# 5107
ISRIB	Sigma-Aldrich	Cat# SML0843
Puromycin dihydrochloride	Gibco	Cat# A1113803
Cycloheximide	Merck Millipore	Cat# 239763
Branched 25-kDa polyethylenimine (PEI)	Sigma-Aldrich	Cat# 408727
CelLytic M	Sigma-Aldrich	Cat# C2978
Phosphatase inhibitor cocktail 2	Sigma-Aldrich	Cat# P5726
Phosphatase inhibitor cocktail 3	Sigma-Aldrich	Cat# P0044
Protease inhibitor cocktail	Sigma-Aldrich	Cat# P8340
4x Laemmli sample buffer	Bio-Rad	Cat# 1610747
Critical commercial assays		
Lipofectamine™ 3000 Transfection Reagent	Invitrogen	Cat# L3000001
Qubit™ Protein Assay kit	Invitrogen	Cat# Q33212
Revert 700 Total Protein Stain	LI-COR	Cat# 926-11011

(*Continued on next page*)

Continued

REAGENT or RESOURCE	SOURCE	IDENTIFIER
Deposited data		
Original immunoblots	Mendeley Data Repository	https://doi.org/10.17632/tjtcftj3cf.1
Experimental models: Cell lines		
SH-SY5Y	ATCC	Cat# CRL-2266
U373	Sigma-Aldrich	Cat# 08061901
MO3.13	Cedarlene	Cat# CLU301-P
Recombinant DNA		
pCMV6-AC-mGFP	Origene	Cat# PS100040
pCMV6-AC-mRFP	Origene	Cat# PS100034
Plasmid: EIF2B5-tGFP	Origene	Cat# RG202322
Plasmid: EIF2S1-tGFP	Origene	Cat# RG200368
Plasmid: EIF2B5-mGFP	This work	N/A
Plasmid: EIF2B5-mRFP	This work	N/A
Software and algorithms		
GraphPad Prism 9.2.0	GraphPad	https://www.graphpad.com/
Zeiss Zen 2.3 (Blue edition)	Zeiss	https://www.zeiss.com/
Image Studio™ Lite	LI-COR	https://www.licor.com/bio/image-studio/
Illustrator CS6	Adobe Inc.	https://www.adobe.com/products/illustrator.html
BioRender	BioRender	https://www.biorender.com/

EXPERIMENTAL MODEL AND STUDY PARTICIPANT DETAILS

Human U373 astrocytoma cells were cultured in Minimum Essential Medium (MEM), supplemented with 10% (v/v) heat-inactivated fetal bovine serum (FBS), 1% (w/v) Non-essential amino acids, 1% (w/v) sodium pyruvate, 2 mM L-glutamine and 1% (w/v) penicillin/streptomycin. Human SH-SY5Y dopaminergic neuroblastoma cells were cultured in Dulbecco's modified Eagle's medium:F-12 (DMEM:F-12; 1:1) containing high glucose (3.151 g/L) (Lonza), supplemented with 10% (v/v) heat-inactivated fetal bovine serum (FBS), 2 mM L-glutamine and 1% (w/v) penicillin/streptomycin. Human MO3.13 hybrid primary oligodendrocytes were cultured in high glucose Dulbecco's modified Eagle's medium (DMEM), supplemented with 10% (v/v) heat-inactivated fetal bovine serum (FBS), 2 mM L-glutamine and 1% (w/v) penicillin/streptomycin. All experiments were done with passage number no higher than 25. All media and supplements were purchased from Life Technologies Co. (New York, USA), except when indicated otherwise. All cell lines were maintained at 37°C under 5% CO2 and were routinely tested for contamination with MycoAlert Mycoplasma Detection Kit (Lonza).

METHOD DETAILS

Cell treatments

For acute/transient induction of the ISR, cells were treated with 1 μM thapsigargin (Tg) for 60 min; 3 μg/mL tunicamycin (Tm) for 2h; and 125 μM sodium arsenite (SA) for 30 min. For chronic induction of the ISR, cells were treated with 300 nM Tg for 24h. For acute/transient cellular stress previously challenged with a chronic induction of the ISR, cells were treated with 300 nM Tg for 24h where 1 μM Tg, 3 μg/mL Tm or 125 μM SA were added in the last 1h, 2h and 30 min, respectively. For ISRIB treatment, cells were added with 200 nM ISRIB for 1h. For PERK inhibition treatment, cells were treated with 500 nM GSK2606414 for 1h. As control, cells were treated with vehicle solution (DMSO) with the highest volume and treatment duration depending on its respective experimental setup.

Plasmids

pCMV6-AC-tGFP plasmid vector encoding *EIF2B5* and *EIF2S1* was purchased from OriGene (Rockville, Maryland, USA). The coding open reading frame of *EIF2B5* from the pCMV6-AC-tGFP vector was cloned into an empty pCMV6-AC-mGFP and empty pCMV6-AC-mRFP vectors. The constructs were verified by sequencing.

Transient transfection procedures

U373, SH-SY5Y and MO3.13 cells were seeded at a density of $3x10^5$, $5x10^5$ and $2.5x10^5$ cells, respectively, in a 6-well plate for at least 24 h before transfection. For U373 cells, transient transfection was performed with transfection reagent 25-kDa polyethylenimine, branched (PEI) (1 mg/mL). 1 μg of plasmid DNA was diluted in 100 μL of serum- and antibiotic-free medium and incubated with 4 μg PEI for 10 min.

600 μL of antibiotic-free media was added to the transfection mixture, added to cells, and incubated for 4 h at 37°C. Media was removed and replaced with complete media and incubated for 24-48 h at 37°C prior to confocal imaging. SH-SY5Y and MO3.13 cells were transfected with Lipofectamine 3000 according to the manufacturer's instructions.

Immunoblotting

$5x10^5$ cells were cultured on 6-well plates. Whole-cell protein lysates were prepared in CelLytic M lysis buffer with 1% protease/phosphatase inhibitors and other supplements (17.5 mM β-glycerophosphate, 1 mM PMSF, 10 mM NaF). Lysates were incubated on ice for 10 min and centrifuged (13,000 rpm, 10 min, 4°C) to remove cellular debris. Protein concentrations were determined with Qubit Protein Assay Kit and subjected to SDS-PAGE electrophoresis. For western blots, samples were run on 7.5 or 10% polyacrylamide gel and transferred using Trans-Blot Turbo Mini-nitrocellulose Transfer packs (Bio-Rad) on a Trans-Blot Turbo apparatus. When necessary, membranes were subjected to Revert Total Protein Stain following manufacturer's instructions. Membranes were blocked in 5% milk or 5% BSA and probed with primary antibodies diluted in 5% milk or 5% BSA, overnight at 4°C. The following antibodies were used: eIF2α (1:500), phosho-eIF2α[ser51] (1:500), PERK (1:1000), GADD34 (1:500), CHOP (1:1000), ATF4 (1:750), GAPDH (1:5,000). Membranes were then washed 3 times for 5 min/each in TBST, followed by probing with secondary antibodies diluted in 5% milk or 5% BSA in TBST for 1h at RT: goat-*anti*-rabbit IRDye 680RD (1:10,000) and goat-*anti*-mouse IRDye 800CW (1:10,000) and washed 3 times for 5 min/each in TBST. Membranes were visualised and quantified on a LiCor Odyssey Scanner with Image Studio Lite software.

Puromycin incorporation assay

For puromycin integration, 91 μM puromycin dihydrochloride was added to media 5 min prior to harvesting and incubated at 37°C. Cells were washed twice with ice-cold PBS supplemented with 355μM cycloheximide, lysed and immunoblotted as described previously. Primary puromycin-specific antibody (1:500) was used to detect puromycinylated proteins. GAPDH was used as loading control.

Immunocytochemistry

22 × 22 mm squared glass coverslips (Sigma-Aldrich) were rinsed with 100% IMS (Fisher Scientific), added to 6-well plates, and left until IMS fully evaporated. Cells were seeded and transfected as described previously. U373 and SH-SY5Y cells were fixed in ice-cold methanol (Fisher Scientific) at −20°C for 15 min, and MO3.13 cells in 4% (w/v) paraformaldehyde (Alfa Aesar) at RT for 20 min. For methanol fixation, cell membranes were washed with PBS supplemented with 0.5% (v/v) Tween 20 (PBST), 3 times for 3 min and then blocked in PBS supplemented with 1% (w/v) bovine serum albumin (BSA) for 60 min at RT, or overnight at 4°C, under gentle shaker. For paraformaldehyde fixation, cells were washed 3 times with PBST for 3 min, permeabilized with 0.1% (v/v) X-Triton for 5 min at RT and blocked in 1% (w/v) BSA in PBST for 60 min at RT or overnight at 4°C, under gentle shaker. Cell membranes were probed with primary antibodies diluted in 1% (w/v) BSA in PBS, overnight at 4°C under gentle shaker, as following: eIF2Bα (1:25), eIF2Bβ (1:25), eIF2Bγ (1:50), eIF2Bδ (1:50), eIF2Bε (1:25), anti-GFAP (1:500), anti-MBP (1 μg/mL) and anti-NeuN (0.1 μg/mL). Cells were then washed 3 times with PBST for 5 min, followed by probing with the appropriate host species Alexa Fluor conjugated secondary antibody, diluted in 1% (w/v) BSA in PBS (1:500), for 60 min at RT. Following secondary antibody incubation, cells were washed with PBST, 3 times for 5 min, and mounted with ProLong Gold Antifade Mountant with DAPI (Invitrogen, Thermo Fisher Scientific). Cells were visualised on a Zeiss LSM 800 confocal microscope.

Confocal imaging and fluorescence recovery after photo bleaching (FRAP)

Imaging was performed using a Zeiss LSM 800 confocal microscope combined with Zeiss ZEN 2.3 (blue edition) software for data processing and analysis. Both 40x and 63× plan-apochromat oil objectives were used and a laser with maximum output of 10 mW at 0.2% (488 nm) and 5.0% (561 nm) laser transmissions. Fluorescence crosstalk was minimal and bleed-through was not observed. Image acquisition was performed by orthogonal projection of a z stack of automatically calculated increments for complete single cell imaging. FRAP analysis was performed to quantify the shuttling rate of eIF2 through localised eIF2B as described in the methodology by (Hodgson et al., 2019). FRAP experiments were carried out by live cell imaging in an incubation chamber with appropriate temperature and CO_2 levels. Specific areas containing an entire cytoplasmic eIF2α-tGFP foci were manually marked for bleaching using 23 iterations at 100% laser transmission (488 nm argon laser). Pre-bleaching image and intensity of targeted foci (ROI – region of interest) was captured followed by 44 images captured every 151 ms for a total of 7.088 s. In-cell fluorescence intensity was captured to normalise against ROI. Out-of-cell fluorescence, or background intensity (B), was measured and subtracted from ROI and T values to provide corrected measurements. Normalised data was fitted to a one-phase association curve using GraphPad Prism to quantify rate of recovery. The relative percentage of eIF2 recovery was determined as the plateau of the normalised FRAP curve.

QUANTIFICATION AND STATISTICAL ANALYSIS

All statistical assessments were made in GraphPad Prism 9.2.0 software, with a significance at $p < 0.05$. All data is presented as means ± standard errors of the mean (s.e.m.). Data was subjected to the Shapiro-Wilk normality test. If parametric, data was analyzed by one-way ANOVA test for comparison of three or more groups followed by Tukey's correction post-hoc test. If non-parametric, data was analyzed by Kruskal-Wallis test for comparison of three or more groups followed by Dunn's correction post-hoc test.